J|A|C|S ARTICLES

Published on Web 10/12/2009

Deuterium Spin Probes of Backbone Order in Proteins: ^{2}H NMR Relaxation Study of Deuterated Carbon α Sites

Devon Sheppard,[‡] Da-Wei Li,[§] Rafael Brüschweiler,[§] and Vitali Tugarinov*,[‡]

Department of Chemistry and Biochemistry, University of Maryland, College Park, Maryland 20742, and Chemical Sciences Laboratory, Department of Chemistry and Biochemistry and National High Magnetic Field Laboratory, Florida State University, Tallahassee, Florida 32306

Received July 30, 2009; E-mail: vitali@umd.edu

Abstract: ^{2}H spin relaxation NMR experiments to study the dynamics of deuterated backbone α-positions, D^α, are developed. To date, solution-state ^{2}H relaxation measurements in proteins have been confined to side-chain deuterons—primarily $^{13}CH_2D$ or $^{13}CHD_2$ methyl groups. It is shown that quantification of ^{2}H relaxation rates at D^α backbone positions and the derivation of associated order parameters of $C^\alpha-D^\alpha$ bond vector motions in small [U-^{15}N,^{13}C,^{2}H]-labeled proteins is feasible with reasonable accuracy. The utility of the developed methodology is demonstrated on a pair of proteins—ubiquitin (8.5 kDa) at 10, 27, and 40 °C, and a variant of GB1 (6.5 kDa) at 22 °C. In both proteins, the D^α-derived parameters of the global rotational diffusion tensor are in good agreement with those obtained from ^{15}N relaxation rates. Semiquantitative solution-state NMR measurements yield an average value of the quadrupolar coupling constant, QCC, for D^α sites in proteins equal to 174 kHz. Using a uniform value of QCC for all D^α sites, we show that $C^\alpha-D^\alpha$ bond vectors are motionally distinct from the backbone amide N−H bond vectors, with ^{2}H-derived squared order parameters of $C^\alpha-D^\alpha$ bond vector motions, $S^2_{C\alpha D\alpha}$, on average slightly higher than their N−H amides counterparts, S^2_{NH}. For ubiquitin, the ^{2}H-derived backbone mobility compares well with that found in a 1-μs molecular dynamics simulation.

Introduction

It is becoming increasingly apparent that protein function is often predicated upon the character and amplitudes of motions undergone by protein structures—that is, molecular dynamics.[1−4] As a result, the past decade has witnessed an upsurge in the development of both experimental and theoretical approaches for studying motional processes in proteins on a variety of time scales. NMR spectroscopy is a particularly powerful experimental method for studying dynamics in proteins because it provides site-specific information that covers a wide range of motional time scales.[5−12] The amide ^{15}N nuclei are the most commonly used spin probes of backbone motions in proteins, and ^{15}N-based NMR relaxation studies of fast dynamics at backbone ^{15}N−^{1}H amide positions of small- to medium-sized proteins are now largely routine.[5,13]

The popularity of ^{15}N as a nuclear spin probe of motional processes in backbones of proteins stems from the ease and affordability of selective incorporation of ^{15}N into backbone amide positions (without concomitant ^{13}C-labeling of neighboring nuclear sites) as well as high sensitivity of ^{15}N relaxation measurements.[5,13] The rates of decay of ^{15}N magnetization in amide moieties is expressed as the sum of dipolar (^{15}N−^{1}H) and ^{15}N chemical shielding anisotropy (CSA) contributions.[5,13,14] Quantitative interpretation of conventional ^{15}N NMR relaxation data in terms of microdynamic characteristics of fast (pico- to nanosecond) motions requires, however, prior knowledge of a number of parameters, such as (i) exact ^{15}N−^{1}H bond lengths, (ii) amide ^{15}N CSA values, and (iii) contributions to the relaxation rates due to chemical exchange, R_{ex}, that, in principle, should be quantified independently. Although ^{15}N relaxation rates in small- to medium-sized proteins usually can be measured with high accuracy, uncertainties in any or all of the above parameters lead to ambiguity in the obtained measures of backbone order expressed as generalized order parameters (amplitudes) of N−H bond vector fluctuations, S_{NH}.[15,16] That is why significant efforts have been dedicated recently to development of NMR methodology that would provide "ex-

[‡] University of Maryland.
[§] Florida State University.

(1) Fersht, A. *Structure and Mechanism in Protein Science*; Freeman & Co.: New York, 2002.
(2) Frauenfelder, H.; Sligar, S. G.; Wolynes, P. G. *Science* **1991**, *254*, 1598–1603.
(3) Dobson, C. M.; Karplus, M. *Curr. Opin. Struct. Biol.* **1999**, *9*, 92–101.
(4) Karplus, M.; Kuriyan, J. *Proc. Natl. Acad. Sci. U.S.A.* **2005**, *102*, 6679–6685.
(5) Peng, J. W.; Wagner, G. *Methods Enzymol.* **1994**, *239*, 563–596.
(6) Palmer, A. G. *Curr. Opin. Struct. Biol.* **1997**, *7*, 732–737.
(7) Ishima, R.; Torchia, D. A. *Nat. Struct. Biol.* **2000**, *7*, 740–743.
(8) Palmer, A. G.; Kroenke, C. D.; Loria, J. P. *Methods Enzymol.* **2001**, *339*, 204–238.
(9) Kay, L. E. *Nat. Struct. Biol. NMR Suppl.* **1998**, *5*, 513–516.
(10) Palmer, A. G. *Annu. Rev. Biophys. Biomol. Struct.* **2001**, *30*, 129–155.
(11) Fushman, D.; Cowburn, D. *Methods Enzymol.* **2001**, *339*, 109–126.
(12) Korzhnev, D. M.; Billeter, M.; Arseniev, A. S.; Orekhov, V. Y. *Prog. Nucl. Magn. Reson. Spectrosc.* **2001**, *38*, 197–266.
(13) Kay, L. E.; Torchia, D. A.; Bax, A. *Biochemistry* **1989**, *28*, 8972–8979.
(14) Cavanagh, J.; Fairbrother, W. J.; Palmer, A. G.; Rance, M.; Skelton, N. J. *Protein NMR Spectroscopy*; Elsevier Academic Press: New York, 2007.
(15) Lipari, G.; Szabo, A. *J. Am. Chem. Soc.* **1982**, *104*, 4559–4570.
(16) Lipari, G.; Szabo, A. *J. Am. Chem. Soc.* **1982**, *104*, 4546–4559.

change-free" and "CSA-free" amide ^{15}N relaxation data in proteins.[17,18]

In search of a "cleaner" spin probe of backbone order in protein molecules, we designed ^2H-based spin relaxation experiments for the studies of dynamics at deuterated backbone α-positions, D^α. Deuterium relaxation is dominated by a strong and local quadrupolar interaction,[19] and knowledge of only a single parameter, the anisotropy of ^2H quadrupolar tensor or quadrupolar coupling constant (QCC), is needed to quantitatively describe D^α ^2H relaxation data in terms of order parameters of $C^\alpha-D^\alpha$ bond motions, $S_{C\alpha D\alpha}$. Since the seminal introduction of deuterium relaxation measurements to the field of protein NMR by Kay and co-workers,[20] deuterium has been recognized as a particularly favorable probe for the studies of dynamics. Millet et al.[21] and Skrynnikov et al.[22] have demonstrated the utility of deuterium spin probes of side-chain dynamics by the measurement of five relaxation rates per deuteron in $^{13}CH_2D$ methyl groups of a 6.5-kDa protein L. The motional properties of ^{13}CHD methylene positions in N-terminal drk SH3 domain have been studied by ^2H relaxation.[23] Comparisons of ^2H-derived and ^{13}C-derived methyl three-fold axis order parameters (S^2_{axis}) in proteins have been provided.[24,25] To date, however, ^2H relaxation measurements in proteins have been confined to side-chain deuterons, primarily methyl groups of the $^{13}CH_2D$[20,21,26,27] or $^{13}CHD_2$[27,28] variety. We show that the availability of increasingly sensitive NMR instrumentation allows the quantification of ^2H relaxation rates at D^α positions of protein backbones as well as the associated order parameters of $C^\alpha-D^\alpha$ bond vector motions in small [U-^{15}N,^{13}C,^2H]-labeled protein molecules.

The developed NMR methodology has been applied to a pair of small proteins—an 8.5-kDa ubiquitin at three temperatures and a variant of a 6.5-kDa protein GB1. The parameters of the global molecular reorientation can be reproduced using D^α ^2H R_2/R_1 ratios, with the extracted diffusion tensors in good agreement with those derived from ^{15}N data in both proteins. Relying on a number of previous solid-state NMR measurements and our own semiquantitative solution-state results, we propose the use of a uniform QCC value of 174 kHz for D^α sites in proteins. Using this QCC value, it is shown that $C^\alpha-D^\alpha$ bond vectors are motionally distinct from the backbone amide N−H bond vectors. In particular, ^2H-derived $S^2_{C\alpha D\alpha}$ values are similar to, but on average slightly higher than, their ^{15}N-derived S^2_{NH} counterparts. Importantly, D^α rates can sample protein backbone motions that are inaccessible through ^{15}N relaxation measurements. Although for sensitivity reasons the developed methodology is expected to be limited to small protein molecules, the advantages of using ^2H relaxation of D^α sites make it a useful complement to the existing array of NMR techniques for quantitative studies of motional order in proteins.

Materials and Methods

NMR Samples. The following isotopically labeled samples of wild-type human ubiquitin and a variant of GB1 protein were used in this work: (i) [U-^{15}N]-labeled (both proteins), (ii) [U-^{15}N,^{13}C,^2H]-labeled (both proteins), and (iii) a mixture of [U-^{15}N,^{13}C,^2H]-labeled and [U-^{15}N,^{13}C]-labeled GB1. The deuterated samples of both proteins were obtained using [U-^{15}N,^{13}C]-glucose as the main carbon source in the 99.9% D_2O-based *Escherichia coli* media. Since carbon α positions are completely deuterated in proteins obtained using D_2O as the solvent in bacterial medium,[29,30] residual protonation of some aliphatic and aromatic sites is of no consequence for the present study. All samples of GB1 were obtained using a co-expression vector where the sequence of GB1 serves as a removable tag, resulting in the addition of seven residues (-Ser-Ser-Gly-Leu-Val-Pro-Arg) to the C-terminus of the protein.

The [U-^{15}N,^{13}C,^2H]- and [U-^{15}N]-labeled NMR samples of human ubiquitin were 3.2 and 1.0 mM in protein concentration, respectively, and were dissolved in a 20 mM 90% H_2O/10% D_2O sodium phosphate buffer (pH 6.8) containing 0.03% NaN_3 and a cocktail of protease inhibitors. The [U-^{15}N,^{13}C,^2H]- and [U-^{15}N]-labeled samples of GB1 were 5.8 and 1.2 mM in protein concentration, respectively, and were dissolved in a 25 mM 90% H_2O/10% D_2O sodium phosphate buffer (pH 6.5) containing 50 mM NaCl, 0.03% NaN_3, and a cocktail of protease inhibitors. A third sample of GB1 contained a mixture of the [U-^{15}N,^{13}C,^2H]- and [U-^{15}N,^{13}C]-labeled protein in the approximate ratio of 4.5:1 (final concentrations of [U-^{15}N,^{13}C,^2H]- and [U-^{15}N,^{13}C]-GB1 of 4.5 and 1 mM, respectively) and was dissolved in a 25 mM 90% H_2O/10% D_2O sodium phosphate buffer (pH 6.5) as above to enable the measurements of D^α quadrupolar splittings and $^1D_{C\alpha H\alpha}$ residual dipolar couplings (RDCs) in the same protein solution (see below).

Experimental NMR Pulse Sequence Details. Figure 1 shows the pulse schemes that have been designed for the measurements of $R^Q(D_+)$, $R^Q(D_z)$, $R^Q(D_+D_z + D_zD_+)$, and $R^Q(3D_z^2\text{-}2)$ at D^α sites of deuterated proteins. The scheme derives from a gradient sensitivity-enhanced HN(COCA) experiment[31] and involves additional magnetization transfers to and from D^α nuclei whose relaxations are measured by parametrically varying delay T. Insets A and B correspond to the measurement of $R^Q(D_+)$ and $R^Q(D_z)$, respectively. The part of the scheme that is enclosed in a dashed rectangle should be modified, as it is shown in the figure to measure the relaxation of the $D_+D_z + D_zD_+$ $(3D_z^2 - 2)$ elements in insets C (D). All narrow (wide) rectangular pulses are applied with the flip angles of 90° (180°) along the *x*-axis unless indicated otherwise. The $^1H(^2H;^{15}N)$ carriers are positioned at 4.7(4.5;119) ppm. The ^{13}C carrier is placed at 177 ppm, switched to 57 ppm before the first 90° $^{13}C^\alpha$ pulse (after gradient g5), and switched back to 177 ppm after the last 90° $^{13}C^\alpha$ pulse (after gradient g9). ^{15}N WALTZ-16[32] decoupling during acquisition is achieved using a 1.25 kHz field, while ^2H GARP-1[33] decoupling uses a 0.9 kHz field. ^2H decoupling is interrupted for the application of gradients g6 and g8 (insets A and B).[34] SEDUCE[35] $^{13}C^\alpha$ decoupling is implemented

(17) Hansen, D. F.; Yang, D.; Feng, H.; Zhou, Z.; Wiesner, S.; Bai, Y.; Kay, L. E. *J. Am. Chem. Soc.* **2007**, *129*, 11468–11479.
(18) Xu, J.; Millet, O.; Kay, L. E.; Skrynnikov, N. R. *J. Am. Chem. Soc.* **2005**, *127*, 3220–3229.
(19) Abragam, A. *Principles of Nuclear Magnetism*; Clarendon Press: Oxford, 1961.
(20) Muhandiram, D. R.; Yamazaki, T.; Sykes, B. D.; Kay, L. E. *J. Am. Chem. Soc.* **1995**, *117*, 11536–11544.
(21) Millet, O.; Muhandiram, D. R.; Skrynnikov, N. R.; Kay, L. E. *J. Am. Chem. Soc.* **2002**, *124*, 6439–6448.
(22) Skrynnikov, N. R.; Millet, O.; Kay, L. E. *J. Am. Chem. Soc.* **2002**, *124*, 6449–6460.
(23) Yang, D.; Mittermaier, A.; Mok, Y. K.; Kay, L. E. *J. Mol. Biol.* **1998**, *276*, 939–954.
(24) Ishima, R.; Petkova, A. P.; Louis, J. M.; Torchia, D. A. *J. Am. Chem. Soc.* **2001**, *123*, 6164–6171.
(25) Lee, A. L.; Flynn, P. F.; Wand, A. J. *J. Am. Chem. Soc.* **1999**, *121*, 2891–2902.
(26) Millet, O.; Mittermaier, A.; Baker, D.; Kay, L. E. *J. Mol. Biol.* **2003**, *329*, 551–563.
(27) Tugarinov, V.; Ollerenshaw, J. E.; Kay, L. E. *J. Am. Chem. Soc.* **2005**, *127*, 8214–8225.
(28) Tugarinov, V.; Kay, L. E. *J. Am. Chem. Soc.* **2006**, *128*, 12484–12489.
(29) Rosen, M. K.; Gardner, K. H.; Willis, R. C.; Parris, W. E.; Pawson, T.; Kay, L. E. *J. Mol. Biol.* **1996**, *263*, 627–636.
(30) Gardner, K. H.; Rosen, M. K.; Kay, L. E. *Biochemistry* **1997**, *36*, 1389–1401.
(31) Bax, A.; Ikura, M. *J. Biomol. NMR* **1991**, *1*, 99–104.
(32) Shaka, A. J.; Keeler, J.; Frenkiel, T.; Freeman, R. *J. Magn. Reson.* **1983**, *52*, 335–338.
(33) Shaka, A. J.; Barker, P. B.; Freeman, R. *J. Magn. Reson.* **1985**, *64*, 547–552.
(34) Kay, L. E. *J. Am. Chem. Soc.* **1993**, *115*, 2055–2057.
(35) McCoy, M. A.; Mueller, L. *J. Magn. Reson.* **1992**, *98*, 674–679.

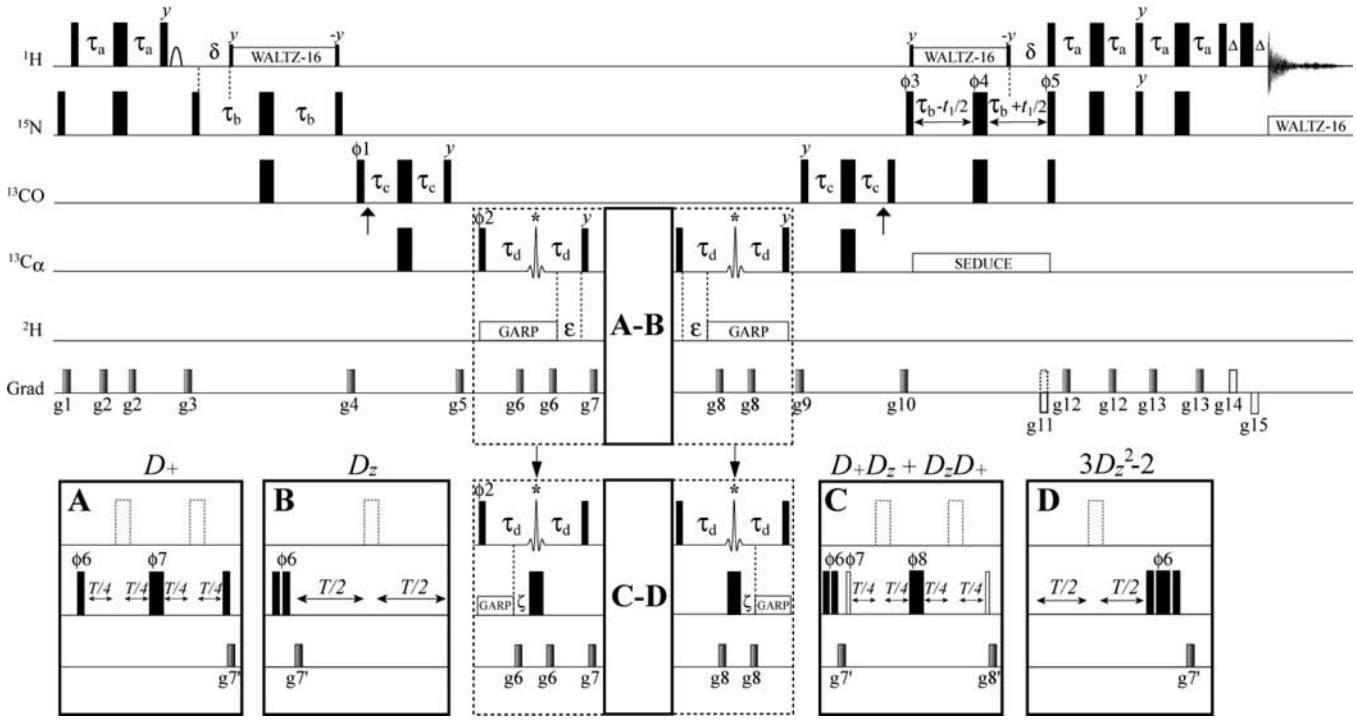

Figure 1. HN(COCA)D pulse scheme for the measurement of relaxation rates of α-deuterons in proteins. See Materials and Methods for the pulse sequence details.

with 300 μs seduce-shaped pulses applied at $^{13}C^{\alpha}$ frequency by phase modulation of the carrier.[36,37] ^{1}H WALTZ-16[32] decoupling is applied with a 7 kHz field. All ^{1}H, ^{2}H, and ^{15}N pulses are applied with maximum possible power, while 90° (180°) ^{13}C pulses shown with filled rectangles are applied with a field strength of $\Delta/\sqrt{15}$ ($\Delta/\sqrt{3}$), where Δ is the difference in hertz between the $^{13}C^{\alpha}$ and ^{13}CO chemical shifts.[38] Vertical arrows at the beginning and end of $2\tau_c$ periods indicate the position of the ^{13}CO Bloch−Siegert shift compensation pulses.[38] $^{13}C^{\alpha}$-shaped pulses marked with asterisks in the middle of $2\tau_d$ periods are 350 μs RE-BURP[39] pulses centered at 43 ppm by phase modulation of the carrier and cover the range of all ^{13}C aliphatic chemical shifts. The ^{2}H pulses shown with open rectangles in inset C have a flip angle of 45°. The $^{13}C^{\alpha}$ pulses shown with open dashed rectangles (insets A−C) are optional. All the experiments described in this work were performed with these pulses included. The ^{1}H pulse shown with an arc (preceding gradient g3) is implemented as a water-selective 1.5 ms pulse of rectangular shape. Delays are $\tau_a = 2.7$ ms, $\tau_b = 12.5$ ms, $\tau_c = 4.5$ ms, $\tau_d = 14$ ms, $\delta = 5.4$ ms, $\varepsilon = 11$ ms, $\zeta = 7$ ms, and $\Delta = 0.4$ ms. The phase cycle is as follows: $\phi1 = x,-x$; $\phi2 = 2(x),2(-x)$ (insets A,B) and $4(x),4(-x)$ (insets C,D); $\phi3 = x$; $\phi4 = 8(x),8(-x)$; $\phi5 = x$; $\phi6 = 4(x),4(-x)$ (insets A,C) and 2(0°),2(45°),2(90°),2(135°) (inset D); $\phi7 = 2(x),2(y),2(-x),2(-y)$ (inset A) and $8(x),8(-x)$ (inset C); $\phi8 = x,-x,y,-y$ (inset C); rec. $= 2(x,-x)$, $2(-x,x)$ (inset A), $x,2(-x),x,-x,2(x),-x$ (inset B), $x,2(-x),x,-x,2(x),-x,-x,2(x)$, $-x,x,2(-x),x$ (inset C), and $x,2(-x),x,-x,2(x),-x$ (inset D). Quadrature detection in t_1 is achieved via the Rance−Kay scheme: for each t_1 value a pair of spectra is recorded with $\phi5 = x$, g11 and $\phi5 = -x$, −g11 and manipulated post-acquisition.[40,41] The phase $\phi3$ is inverted for each t_1 point.[42] Durations and strengths of pulsed-field gradients in units of (ms; G/cm) are as follow: g1 = (1; 15); g2 = (0.25; 5); g3 = (1.2; 12); g4 = (0.5; 8); g5 = (0.6; 10); g6 = (0.3; 5); g7 = (0.7; 15); g8 = (0.35; 5); g9 = (0.5; 12); g10 = (0.4; 10); g11 = (1.25; 20); g12 = (0.25; 8); g13 = (0.3; 5); g14 = (0.0625; 20); g15 = (0.0625; −20); g7′ = (0.6; 10); g8′ = (0.8; 12).

D^{α} and ^{15}N Relaxation Measurements. All ^{2}H and ^{15}N spin relaxation experiments were performed on a 600 MHz Bruker Avance III spectrometer equipped with a room-temperature triple-resonance z-gradient probe. NMR data sets recorded with the pulse scheme of Figure 1 (D^{α}, [U-^{15}N,^{13}C,^{2}H]-labeled samples) comprised [512, 40] complex points in the [^{1}HN, ^{15}N] dimensions, with corresponding acquisition times of [64 ms, 24 ms]. Typically, a recovery delay of 1.5 s was used along with 128 scans/FID, giving rise to net acquisition times of ∼4.8 h/experiment. $R^Q(D_+)$ rates in ubiquitin samples were recorded with parametrically varied delays T (Figure 1, inset A) of (0.02; 0.2; 0.4; 0.6; 0.8; 1.2; 1.6) ms, (0.02; 0.3; 0.6; 0.9; 1.2; 1.6; 2.0) ms, and (0.02; 0.2; 0.4; 0.6; 0.8; 1.2; 1.6) ms at 10, 27, and 40 °C, respectively, while $R^Q(D_z)$ rates were recorded with parametrically varied delays T (Figure 1, inset B) of (0.02; 2.0; 4.0; 6.0; 8.0; 10.0; 12.0; 14.0) ms, (0.02; 1.0; 2.0; 3.0; 4.0; 6.0; 8.0; 10.0) ms, and (0.02; 1.0; 2.0; 3.0; 4.0; 5.0; 6.0; 8.0) ms at 10, 27, and 40 °C. $R^Q(D_+)$, $R^Q(D_z)$, $R^Q(D_+D_z+D_zD_+)$, and $R^Q(3D_z^2\text{-}2)$ relaxation rates of α deuterons in GB1 were measured at 22 °C using delays T of (0.02; 0.2; 0.4; 0.6; 0.8; 1.2; 1.6; 2.0) ms, (0.02; 2.0; 4.0; 6.0; 8.0; 10.0; 13.0) ms, (0.02; 0.2; 0.4; 0.6; 0.8; 1.2; 1.6; 2.0) ms, and (0.02; 1.0; 2.0; 3.0; 4.0; 6.0; 8.0; 10.0) ms, respectively. All NMR spectra were processed using the NMRPipe/NMRDraw suite of programs[43] and associated software. Rates were obtained by fitting peak intensities to a single-exponential function of the form $I = I_0 \exp(-RT)$, where I is the measured intensity and R is the relaxation rate. Errors in peak intensities were estimated from duplicate measurements or from the noise-floor level of the spectra, whichever was higher, and

(36) Patt, S. L. *J. Magn. Reson.* **1992**, *96*, 94–102.
(37) Boyd, J.; Soffe, N. *J. Magn. Reson.* **1989**, *85*, 406–413.
(38) Kay, L. E.; Ikura, M.; Tschudin, R.; Bax, A. *J. Magn. Reson.* **1990**, *89*, 496–514.
(39) Geen, H.; Freeman, R. *J. Magn. Reson.* **1991**, *93*, 93–141.
(40) Kay, L. E.; Keifer, P.; Saarinen, T. *J. Am. Chem. Soc.* **1992**, *114*, 10663–10665.
(41) Schleucher, J.; Sattler, M.; Griesinger, C. *Angew. Chem., Int. Ed. Engl.* **1993**, *32*, 1489–1491.
(42) Marion, D.; Ikura, M.; Tschudin, R.; Bax, A. *J. Magn. Reson.* **1989**, *85*, 393.
(43) Delaglio, F.; Grzesiek, S.; Vuister, G. W.; Zhu, G.; Pfeifer, J.; Bax, A. *J. Biomol. NMR* **1995**, *6*, 277–293.

subsequently propagated to the errors in the extracted rates using Monte Carlo analysis.[44] The estimated errors in $R^Q(D_+)$ ($R^Q(D_z)$) measurements are on the order of 2.0% (1.5%) on average in ubiquitin.

^{15}N $R_{1\rho}$, R_1 and ^{1}H$-^{15}$N NOE measurements on [U-^{15}N]-labeled samples of both proteins were performed using standard procedures.[45,46] Typically, NMR data sets comprised [512, 64] complex points in the [^{1}HN, ^{15}N] dimensions with corresponding acquisition times of [64 ms, 38 ms]. Recovery delays of 1.0 and 4.3 s (including a 2 s presaturation period) for ^{15}N $R_{1\rho}$, R_1, and ^{1}H$-^{15}$N NOE measurements, respectively, along with 16 scans/FID gave rise to respective net acquisition times of ~0.7 and 2.5 h/experiment. The spin-lock field strength of 1.9 kHz was used in ^{15}N $R_{1\rho}$ measurements. $R_{1\rho}$ data were subsequently corrected for resonance offset to obtain ^{15}N R_2 rates.[5] Error analysis of peak intensities and the extracted relaxation rates closely followed the procedure used for ^{2}H relaxation measurements at D$^\alpha$ positions.

The relaxation rates of $N_zC'_zC^\alpha_z$ three-spin order, $R(N_zC'_zC^\alpha_z)$, were measured using a pulse scheme derived from the gradient sensitivity-enhanced HN(COCA) experiment[31] using the same acquisition parameters as for ^{2}H relaxation measurements. A recovery delay of 1.0 s was used, along with 16 scans/FID, giving rise to net acquisition times of ~30 min/experiment. Relaxation delays T of (0.01; 50; 100; 150; 200; 300; 350; 400; 450; 500; 600) ms were typically used for both proteins at all temperatures. The extracted $R(N_zC'_zC^\alpha_z)$ rates were subsequently subtracted from the obtained D$^\alpha$ R^Q [D] rates before analysis (see text).

Data Analysis. The relaxation rates of ^{2}H transverse and longitudinal magnetization are given by[19]

$$R^Q(D_+) = R_2^Q = \frac{\pi^2}{20}\left(\frac{e^2qQ}{h}\right)^2[9J(0) + 15J(\omega_D) + 6J(2\omega_D)] \quad (1)$$

$$R^Q(D_z) = R_1^Q = \frac{3\pi^2}{10}\left(\frac{e^2qQ}{h}\right)^2[J(\omega_D) + 4J(2\omega_D)] \quad (2)$$

where (e^2qQ/h) is the quadrupolar coupling constant (QCC) and $J(\omega_D)$ is the spectral density function evaluated at ω_D frequency. A uniform value of QCC = 174 kHz has been used for α deuterons in this work. It is usually assumed that the ^{2}H electric field gradient tensor is axially symmetric with its principal axis parallel to the direction of the deuteron bond, so that only the anisotropy of the tensor, (e^2qQ/h) = QCC, enters into eqs 1 and 2. Indeed, the asymmetry values of the ^{2}H tensor, η, in aliphatic deuterons are known to be <0.04.[47,48] If the assumption of axial symmetry is dropped, the relaxation rates in eqs 1 and 2 above should be multiplied by $(1 + \eta^2/3)$, which would contribute <0.06% to $R(D_+)$ and $R(D_z)$. Clearly, such small contributions are well within the errors of the relaxation rate measurements and can be safely neglected.

All ^{2}H data were analyzed using the following Lipari−Szabo model-free spectral density function for the axially symmetric molecular tumbling,[15,16,49]

$$J(\omega) = S^2_{C\alpha D\alpha}\left(\frac{A_1\tau_1}{1 + (\omega\tau_1)^2} + \frac{A_2\tau_2}{1 + (\omega\tau_2)^2} + \frac{A_3\tau_3}{1 + (\omega\tau_3)^2}\right) + (1 - S^2_{C\alpha D\alpha})\frac{\tau'}{1 + (\omega\tau')^2} \quad (3)$$

where $S_{C\alpha D\alpha}$ is the generalized order parameter describing the fluctuations of C$^\alpha-$D$^\alpha$ bond vectors, $A_1 = (3/4)\sin^4(\alpha)$, $A_2 = 3\sin^2(\alpha)\cos^2(\alpha)$, $A_3 = [(3/2)\cos^2(\alpha) - 0.5]^2$, $\tau_1 = (4D_{||} + 2D_\perp)^{-1}$, $\tau_2 = (D_{||} + 5D_\perp)^{-1}$, $\tau_3 = (6D_\perp)^{-1}$, $D_{||}$ and $D_\perp$ are the parallel and perpendicular components of the molecular diffusion tensor, α is the angle between the C$^\alpha-$D$^\alpha$ bond vector (assumed collinear with the C$^\alpha-$H$^\alpha$ bond vector in protein structures) and the unique diffusion axis, and $1/\tau' = 1/\tau_f + 1/\tau_{c,eff}$ with $\tau_{c,eff} = (2D_{||} + 4D_\perp)^{-1}$ the effective correlation time of overall rotation and τ_f the correlation time of fast local motions. Direction cosines for the C$^\alpha-$H$^\alpha$ vectors of ubiquitin and GB1 were obtained from the X-ray structures with the respective PDB accession codes 1ubq[50] and 2qmt.[51]

Diffusion tensors were estimated by minimization of the error function χ^2, expressed as

$$\chi^2 = \sum_{i=1}^{N}\left[\frac{(R_2^{expt}/R_1^{expt})_i - (R_2^{calc}/R_1^{calc})_i}{(\sigma_{R_2/R_1})_i}\right]^2 \quad (4)$$

where the summation extends over all sites included in analysis, R_2^{expt} and R_1^{expt} are the experimentally measured ^{2}H/^{15}N rates, R_2^{calc} and R_1^{calc} are the rates calculated using diffusion tensor parameters (eq 3) and the expressions for R_2^Q, R_1^Q (eqs 1 and 2)/^{15}N R_2, R_1 rates, and σ_{R_2/R_1} is the uncertainty in the experimental R_2/R_1 ratios. A fit to a fully anisotropic diffusion tensor[52] was not warranted for either protein because of relatively high errors in extracted D$^\alpha$ R^Q[D] relaxation rates that preclude a statistically significant differentiation between the axially symmetric and fully anisotropic models. The diffusion tensor parameters obtained by minimization of χ^2 (eq 4) are sensitive to the choice of residues whose dynamics is properly described by the first term of eq 3. Therefore, in both proteins only the residues in the secondary structure elements were used. Likewise, the residues with missing coordinates (C-terminus of GB1), ^{1}H$-^{15}$N NOE < 0.6, and the residues undergoing chemical exchange (^{15}N data only) were excluded from analysis. Errors in the fitted diffusion parameters (polar angles θ, φ describing the orientation of the unique axis of the diffusion tensor with respect to the inertial frame, and $D_{||}$, $D_\perp$) were estimated using 300 Monte Carlo simulations[44] with random additions of experimental errors to the measured rates. The standard deviations in the fitted parameters were used as uncertainties in diffusion parameters.

D$^\alpha$ (^{15}N) relaxation rates were interpreted in terms of motional parameters using their corresponding ^{2}H (^{15}N)-derived diffusion tensor characteristics. Motional parameters of D$^\alpha$ sites, $S^2_{C\alpha D\alpha}$, and the corresponding τ_f values were obtained by fitting the ^{2}H relaxation data to the corresponding expressions for relaxation rates (eqs 1 and 2) using eq 3 for the spectral density function (see Results and Discussion), whereas the motional parameters of N−H bond vectors, S^2_{NH} and τ_f, were obtained using the program Dynamics[53,54] that models ^{15}N relaxation data, selecting for the appropriate motional model (that can be different from the simplest form of eq 3) on the basis of statistical criteria. ^{15}N relaxation data were analyzed with standard expressions for ^{15}N relaxation in ^{15}N$-^1$H spin pairs. ^{15}N R_2, R_1 and ^{1}H$-^{15}$N NOE data were included in the analysis that used the spectral density function of eq 3, where the squared order parameter describing the fluctuations of the backbone amide N−H bond vector, S^2_{NH}, was used instead of $S^2_{C\alpha D\alpha}$ together

(44) Kamith, U.; Shriver, J. W. *J. Biol. Chem.* **1989**, *264*, 5586–5592.
(45) Farrow, N. A.; Muhandiram, R.; Singer, A. U.; Pascal, S. M.; Kay, C. M.; Gish, G.; Shoelson, S. E.; Pawson, T.; Forman-Kay, J. D.; Kay, L. E. *Biochemistry* **1994**, *33*, 5984–6003.
(46) Ferrage, F.; Piserchio, A.; Cowburn, D.; Ghose, R. *J. Magn. Reson.* **2008**, *192*, 302–313.
(47) Wooten, J. B.; Savitsky, G. B.; Jacobus, J.; Beyerlein, A. L.; Emsley, J. W. *J. Chem. Phys.* **1979**, *70*, 438–442.
(48) Schramm, S.; Oldfield, E. *Biochemistry* **1983**, *22*, 2908–2913.
(49) Wöessner, D. E. *J. Chem. Phys.* **1962**, *37*, 647–654.
(50) Vijay-Kumar, S.; Bugg, C. E.; Cook, W. J. *J. Mol. Biol.* **1987**, *194*, 531–544.
(51) Frericks-Schmidt, H. L.; Sperling, L. J.; Gao, Y. G.; Wylie, B. J.; Boettcher, J. M.; Wilson, S. R.; Rienstra, C. M. *J. Phys. Chem. B* **2007**, *111*, 14362–14369.
(52) Tjandra, N.; Feller, S. E.; Pastor, R. W.; Bax, A. *J. Am. Chem. Soc.* **1995**, *117*, 12562–12566.
(53) Fushman, D.; Cahill, S.; Cowburn, D. *J. Mol. Biol.* **1997**, *266*, 173–194.
(54) Hall, J. B.; Fushman, D. *J. Am. Chem. Soc.* **2006**, *128*, 7855–7570.

with the corresponding N−H direction cosines. The N−H bond distance of 1.02 Å and a uniform ^{15}N CSA of −170 ppm were used in all calculations.

D^α Quadrupolar Splitting and $^1D_{C\alpha H\alpha}$ Measurements in Oriented GB1. Analysis of D^α QCC closely followed the work of Mittermaier and Kay, where QCC values were determined for methyl deuterons using the ratios of quadrupolar splittings, ν_Q, and $^{13}C^{methyl}-^{13}C$ RDCs measured in an oriented protein.[55] The same approach can be used for α deuterons provided that $^1D_{C\alpha H\alpha}$ RDCs are measured in the same sample. To enable the measurements of D^α splittings and $^1D_{C\alpha H\alpha}$ RDCs in the same protein sample, a mixture of [U-^{15}N,^{13}C,^2H]-labeled and [U-^{15}N,^{13}C]-labeled GB1 was used (see NMR Samples, above). The use of the same sample with two different labeling schemes (one having ^2H nuclei and the other ^1H nuclei at α positions) ensures that the alignment characteristics and dynamical properties are exactly the same for the ν_Q and $^1D_{C\alpha H\alpha}$ measurements. The "mixed" GB1 sample was aligned in 18 mg/mL pf1 bacteriophage[56] (quadrupolar D_2O splitting of 24.7 Hz). $^1D_{C\alpha H\alpha}$ RDCs were obtained using the HNCO-type experiment of Yang et al.[57] modified to eliminate the resonances of $^{13}C^\alpha$ nuclei attached to deuterons arising from the (more concentrated) [U-^{15}N,^{13}C,^2H]-labeled protein. This experiment allows for convenient measurements of $^1D_{C\alpha H\alpha}$ in H_2O protein solutions by recording the modulation of carbonyl chemical shifts by ($^1J_{C\alpha H\alpha}$ + $^1D_{C\alpha H\alpha}$) couplings (see ref 57). The quadrupolar splittings ν_Q in α deuterons were obtained using the scheme of Figure 1 (inset A) with parametrically varied delays T of (0.02; 0.4; 1.0; 1.1; 1.6; 2.0; 2.3; 2.8; 3.1; 3.5; 4.0; 4.3; 4.8; 5.1; 5.5; 6.0; 6.3; 6.8; 7.1; 7.6; 8.0; 8.6) ms. The $^1D_{C\alpha H\alpha}$ and ν_Q measurements were performed twice and the obtained $\nu_Q/^1D_{C\alpha H\alpha}$ ratios averaged.

Molecular Dynamics Simulations. A 1 μs molecular dynamics (MD) trajectory of ubiquitin was performed as described elsewhere.[58] Briefly, the MD simulation was performed using the AMBER 9 package[59] with the AMBER99SB force field,[60] which was shown previously to accurately reproduce the native state dynamics of ubiquitin.[59,61−63] The SHAKE algorithm[64] was employed to constrain all bonds involving hydrogen atoms, and a time step of 2 fs was used. Non-deuterated ubiquitin was embedded in a cubic box with SPC/E water models, and long-range electronic interactions were handled using the PME method[65] with an 8 Å cutoff. The starting coordinates were taken from the crystal structure of ubiquitin (PDB entry 1ubq), and the simulation was run for 1000 ns at 300 K under NPT conditions after application of standard minimization and heating protocols. The values of $S^2_{C\alpha H\alpha}$ were extracted using the iRED method[66] averaged over time windows of 1 and 5 ns, i.e., on the order of the experimental global tumbling correlation time of ubiquitin.

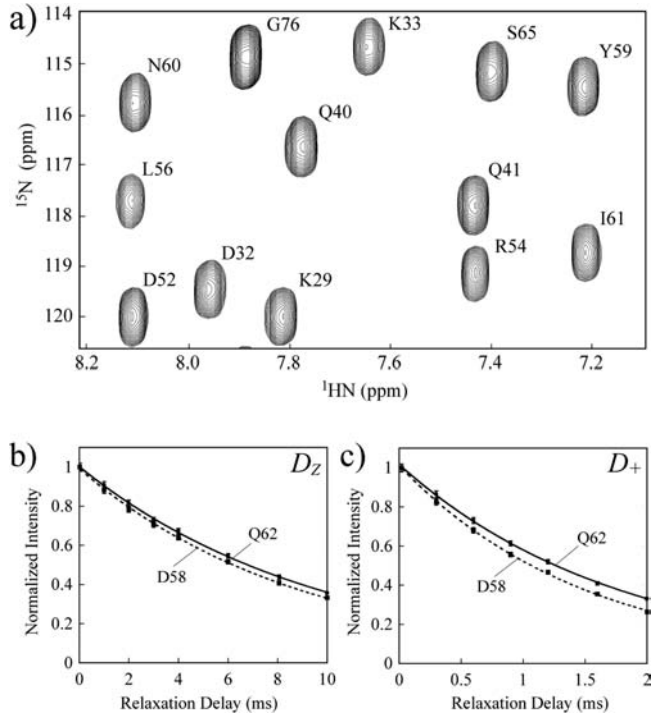

Figure 2. (a) Region of the $^1HN-^{15}N$ correlation map of the [U-^{15}N,^{13}C,^2H]-labeled 3.2 mM ubiquitin (27 °C; 600 MHz) acquired as the first measurement point using the experiment of Figure 1 (inset A, $T = 0$). Assignments of the cross-peaks are shown according to their $^1HN-^{15}N$ frequencies (located at position i if $i - 1$ is the position of the decaying D^α nucleus). Typical decay curves of (b) D_z and (c) D_+ magnetization are shown for Asp[58] (dashed curves) and Gln[62] (solid curves) of ubiquitin.

Results and Discussion

NMR Experiments for the Measurement of ^2H Relaxation Rates at D^α Sites of Proteins. Figure 1 shows the HN(COCA)D experiment used for the measurements of relaxation rates at D^α sites. The pulse scheme is derived from the gradient sensitivity-enhanced HNCOCA experiment[31] with additional delays at $^{13}C^\alpha$ nuclei to allow the magnetization to evolve to and from D^α positions whose relaxation is measured during time period T (see Materials and Methods for the pulse scheme details). The transfer of magnetization can be summarized by

$$^1HN_i \rightarrow {}^{15}N_i \rightarrow {}^{13}CO_{i-1} \rightarrow {}^{13}C^\alpha_{i-1} \rightarrow D^\alpha_{i-1}(T) \rightarrow {}^{13}C^\alpha_{i-1} \rightarrow {}^{13}CO_{i-1} \rightarrow {}^{15}N_i(t_1) \rightarrow {}^1HN_i(t_2) \quad (5)$$

where the transfer from one spin to the next is achieved via one-bond scalar couplings and t_1, t_2 are acquisition times. A series of two-dimensional data sets is recorded as a function of T. The cross-peaks obtained at the frequencies (ω_{Ni}; ω_{HNi}) decay with the relaxation rates of α-deuterons belonging to the previous residue, D^α_{i-1}. A region of such a 2D spectrum recorded on ubiquitin at 27 °C using the pulse scheme of Figure 1 (inset A, $T = 0$) is shown in Figure 2a. Relaxation rates can be extracted directly by fitting the intensity of each correlation to a single-exponential decay curve (Figure 2b,c). Since in glycines the magnetization is transferred from α carbons to *both* α-deuterons, the relaxation rates of the two (nonequivalent) Gly D^α positions cannot be separated. Therefore, glycine residues (i.e., the amide correlations of the residues following glycines)

(55) Mittermaier, A.; Kay, L. E. *J. Am. Chem. Soc.* **1999**, *121*, 10608–10613.
(56) Hansen, M. R.; Mueller, L.; Pardi, A. *Nat. Struct. Biol.* **1998**, *5*, 1065–1074.
(57) Yang, D.; Tolman, J. R.; Goto, N. K.; Kay, L. E. *J. Biomol. NMR* **1998**, *12*, 325–332.
(58) Showalter, S. A.; Brüschweiler, R. *J. Chem. Theory Comput.* **2007**, *3*, 961–975.
(59) Case, D. A.; Cheatham, T. E.; Darden, T.; Gohlke, H.; Luo, R.; Merz, K. M.; Onufriev, A.; Simmerling, C.; Wang, B.; Woods, R. J. *J. Comput. Chem.* **2005**, *26*, 1668–1688.
(60) Hornak, V.; Abel, R.; Okur, A.; Strockbine, B.; Roitberg, A.; Simmerling, C. *Proteins* **2006**, *65*, 712–725.
(61) Showalter, S. A.; Brüschweiler, R. *J. Am. Chem. Soc.* **2007**, *129*, 4158–4159.
(62) Showalter, S. A.; Johnson, E.; Rance, M.; Brüschweiler, R. *J. Am. Chem. Soc.* **2007**, *29*, 14146–14147.
(63) Maragakis, P.; Lindorff-Larsen, K.; Eastwood, M. P.; Dror, R. O.; Klepeis, J. L.; Arkin, I. T.; Jensen, M. O.; Xu, H. F.; Trbovic, N.; Friesner, R. A.; Palmer, A. G.; Shaw, D. E. *J. Phys. Chem. B* **2008**, *112*, 6155–6158.
(64) Ryckaert, J. P.; Ciccotti, G.; Berendsen, H. J. C. *J. Comput. Chem.* **1977**, *23*, 327–341.
(65) Darden, T.; York, D.; Pedersen, L. *J. Chem. Phys.* **1993**, *98*, 10089–10092.
(66) Prompers, J. J.; Brüschweiler, R. *J. Am. Chem. Soc.* **2002**, *124*, 4522–4534.

were excluded from analysis in this work. Likewise, D^{α} relaxation rates of residues preceding prolines cannot be quantified using the experiment of Figure 1. The relaxation rates of proline D^{α} sites can be measured, however, through the amide correlation of the following (non-proline) residue. Although, as shown below, robust measures of backbone dynamics can be obtained from D^{α} relaxation rates, the D^{α} relaxation rate measurements using the scheme of Figure 1 are associated with very significant sensitivity losses compared to conventional ^{15}N relaxation experiments. Taking into account different sample concentrations and acquisition times used for each time point in the $D^{\alpha}/^{15}N$ rate measurements (see Materials and Methods), we estimate that the scheme of Figure 1 is approximately 20 times less sensitive than ^{15}N relaxation experiments, necessitating the use of more concentrated protein samples and/or cryogenically cooled probes for data collection.

D^{α} Relaxation Rates. The R_1 and R_2 relaxation rates of D^{α} nuclei, $R^Q(D_+)$ and $R^Q(D_z)$, have been measured using the experiments shown in insets A and B of Figure 1, respectively. Both experiments measure the relaxation rates of magnetization terms $N_zC'_zC^{\alpha}_z[D]$, where $[D]$ is any deuterium spin operator and A_z is a longitudinal spin operator of nucleus A (carbonyl/carbon-α of residue $i-1$ and nitrogen of residue i). As was the case in the previous deuterium relaxation studies,[20,21,67] it can be shown that, to a very good approximation, $R(N_zC'_zC^{\alpha}_z[D]) = R(N_zC'_zC^{\alpha}_z) + R[D]$, and to obtain a "pure" deuterium relaxation rate it is sufficient to subtract $R(N_zC'_zC^{\alpha}_z)$ from the rates obtained in the experiments of Figure 1. In practice, however, the rates $R(N_zC'_zC^{\alpha}_z)$ are very small compared to $R(N_zC'_zC^{\alpha}_z[D])$. For example, the $R(N_zC'_zC^{\alpha}_zD_+)$ rates measured in ubiquitin vary between 372 and 1042 (321 and 675; 370 and 569) s^{-1} at 10 (27; 40)°C, whereas $R(N_zC'_zC^{\alpha}_zD_z)$ rates in ubiquitin at 10 (27; 40)°C vary between 62 and 115 (90 and 129; 119 and 153) s^{-1}. The rates $R(N_zC'_zC^{\alpha}_z)$, measured as described in Materials and Methods, vary between 2.1 and 2.8 (2.1 and 3.8; 1.9 and 4.0) s^{-1} at 10 (27; 40) °C. Clearly, these rates are within measurement errors of $R(N_zC'_zC^{\alpha}_zD_+)$. This is, however, not necessarily the case for $R(N_zC'_zC^{\alpha}_zD_z)$ measurements, although the corrections remain small. To avoid introduction of systematic errors to the quantified deuterium relaxation rates, the $R(N_zC'_zC^{\alpha}_z)$ values have been subtracted on a residue-specific basis from all measured D^{α} rates in this work. It is important to emphasize that ^2H relaxation of backbone D^{α} sites is completely dominated by the strong quadrupolar interaction, as is also the case in the previous ^2H relaxation studies of $^{13}CH_2D$[20,21,27,68] and $^{13}CHD_2$[27,28] methyl groups and ^{13}CHD methylene sites in proteins,[23] as well as deuterated sugars and bases of RNA molecules.[67] For example, calculations using typical sets of motional parameters obtained in this work for proteins tumbling with isotropic correlation times in the range between 2 and 10 ns show that the maximal contribution of the dipolar interaction of D^{α} deuterons with the directly bonded $^{13}C^{\alpha}$ spins to transverse (longitudinal) D^{α} relaxation rates D_+ (D_z) is 1.0 (0.25) s^{-1}. Evidently, such small contributions are within the errors of D^{α} relaxation rate measurements and can be safely ignored.

Figure 3 shows the profiles of experimental $R^Q(D_z)$ and $R^Q(D_+)$ values obtained in ubiquitin at 10 °C (Figure 3a,d), 27 °C (Figure 3b,e) and 40 °C (Figure 3c,f). For comparison, ^{15}N R_1 and R_2 rate profiles are included in the same plots. The average $R^Q(D_+)$ rates measured at 10 (27; 40) °C in ubiquitin are 880 (597; 500) s^{-1}, whereas average $R^Q(D_z)$ rates are 72 (107; 132) s^{-1}. A higher than average degree of backbone flexibility is manifested in decreased $R^Q(D_+)$ values (i) in the loop between residues Thr^7 and Lys^{11} with average $R^Q(D_+)$ of 813 (571) s^{-1} at 10 (27) °C (Figure 3d,e; the residues in this region could not be reliably quantified at 40 °C); (ii) near the Lys^{48} polymerization site (residues Ala^{46}-Lys^{48}) at all temperatures with average $R^Q(D_+)$ values of 855 (566; 467) s^{-1} at 10 (27; 40) °C; and (iii) at the C-terminus starting from Arg^{72} (Figure 3d−f). These trends are largely mirrored by ^{15}N R_2 rates. Interestingly, $R^Q(D_z)$ profiles show that higher disorder at the C-terminus is accompanied by an increase in $R^Q(D_z)$ rates, while ^{15}N R_1 rates decrease for the same residues (Figure 3a−c; some $R^Q(D_z)$ rates could not be quantified at the C-terminus at 40 °C because of resonance overlap). Notably, the $R^Q(D_z)$ and $R^Q(D_+)$ rates of Gly D^{α} positions have to be excluded from the plots in Figure 3, resulting in a loss of information as some Gly residues in ubiquitin (e.g., Gly^{10} and Gly^{47}) fall in the regions of increased backbone flexibility according to ^{15}N data. It is apparent from Figure 3d−f that chemical exchange on the micro- to millisecond time scale—most notably affecting the amide of Asn^{25} with ^{15}N R_2 rates of 17.2 (8.6; 5.8) s^{-1}, while the average ^{15}N R_2 rates in ubiquitin are 9.0 (6.0; 4.6) s^{-1} at 10 (27; 40) °C—does not affect the D^{α} rates to any significant extent. Large exchange contributions to R_2 relaxation rates can significantly complicate ^{15}N relaxation analysis, while D^{α} relaxation data (with the exception of double-quantum coherences, D_+^2, *vide infra*) remain unaffected by contributions from chemical exchange.

Because the deuteron is a spin 1 nucleus, a total of five relaxation rates can be measured at D^{α} sites. As described by Millet et al.[21] for the case of methyl groups, in addition to "rank-1" coherences D_+ and D_z, the relaxation rates of "rank-2" elements ($D_+D_z + D_zD_+$, $3D_z^2$-2, and D_+^2) can be quantified in the same ^2H site. Indeed, one of the principal advantages of ^2H spin relaxation lies in the possibility to assess the self-consistency of the obtained rates prior to analysis in terms of motional parameters. Jacobsen and co-workers[69] have shown that so long as $J(0) \geq J(\omega_D) \geq J(2\omega_D)$, where $J(\omega_D)$ is the spectral density function evaluated at the ^2H Larmor frequency, ω_D (see Materials and Methods), the following inequalities must hold: $(5/3)R^Q(D_+D_z + D_zD_+) \geq R^Q(D_+) \geq (5/3)R^Q(3D_z^2\text{-}2) \geq R^Q(D_z)$, where the relaxation rates of antiphase ^2H magnetization, $(D_+D_z + D_zD_+)$, and the quadrupolar order, $(3D_z^2\text{-}2)$, are given by

$$R^Q(D_+D_z + D_zD_+) = \frac{\pi^2}{20}\left(\frac{e^2qQ}{h}\right)^2[9J(0) + 3J(\omega_D) + 6J(2\omega_D)] \quad (6)$$

$$R^Q(3D_z^2\text{-}2) = \frac{3\pi^2}{10}\left(\frac{e^2qQ}{h}\right)^2[3J(\omega_D)] \quad (7)$$

The pulse scheme that can be used for $R^Q(D_+D_z + D_zD_+)$ and $R^Q(3D_z^2\text{-}2)$ measurements at D^{α} positions of proteins are shown in insets C and D of Figure 1, respectively. In contrast to ^2H relaxation studies of methyl deuterons, however, the $R^Q(D_+D_z + D_zD_+)$ and $R^Q(3D_z^2\text{-}2)$ measurements at backbone D^{α} sites suffer from very poor sensitivity because of fast ^2H spin-flips occurring during prolonged $^{13}C^{\alpha}_{i-1} \rightarrow D^{\alpha}_{i-1}(T) \rightarrow$

(67) Vallurupalli, P.; Kay, L. E. *J. Am. Chem. Soc.* **2005**, *127*, 6893–6901.
(68) Yang, D.; Kay, L. E. *J. Magn. Reson. Ser. B* **1996**, *110*, 213–218.
(69) Jacobsen, J. P.; Bildsöe, H. K.; Schaumburg, K. *J. Magn. Reson.* **1976**, *23*, 153–164.

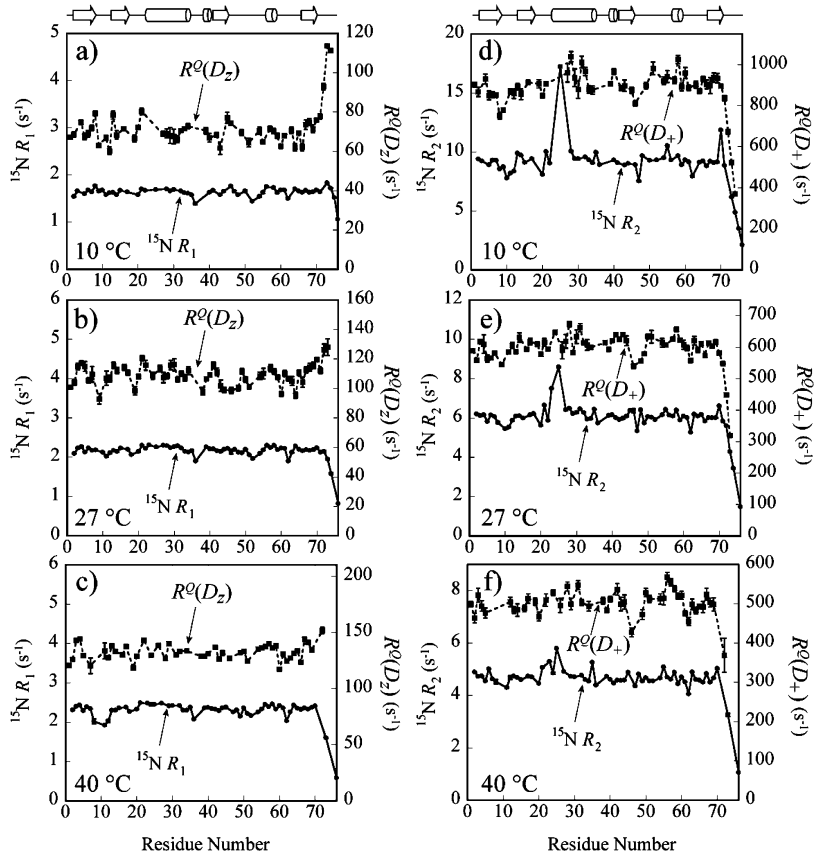

Figure 3. Plots of D^α (shown with black rectangles and dashed lines) and ^{15}N (black circles and solid lines) relaxation rates in ubiquitin as a function of the protein sequence. $R^Q(D_z)$ and ^{15}N R_1 rates are shown at (a) 10, (b) 27, and (c) 40 °C, while $R^Q(D_+)$ and ^{15}N R_2 rates are shown at (d) 10, (e) 27, and (f) 40 °C. The lines connecting the symbols on the plots are intended solely to guide the eye. Schematic representation of the secondary structure of ubiquitin is shown on top: β-sheets are depicted with arrows, while α-helices are represented with cylinders.

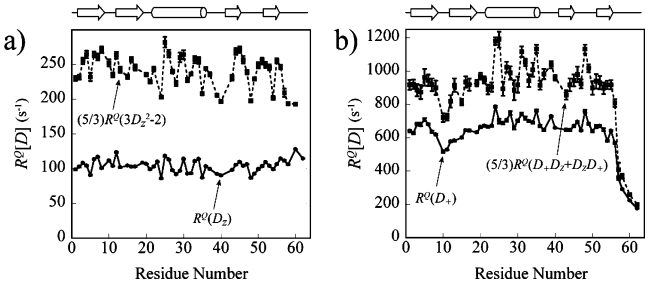

Figure 4. Consistency plots of D^α relaxation rates. (a) $(5/3)R^Q(3D_z^2\text{-}2)$ (shown with black rectangles and dashed lines) and $R^Q(D_z)$ (black circles; solid lines) and (b) $(5/3)R^Q(D_+D_z + D_zD_+)$ (black rectangles; dashed lines) and $R^Q(D_+)$ (black circles; solid lines) rates measured in GB1 at 22 °C (600 MHz) are plotted as a function of GB1 sequence. A schematic representation of the secondary structure of GB1 is shown on top.

$^{13}C^\alpha_{i-1}$ magnetization transfer steps (two time periods $\tau_d + \zeta$ in Figure 1, insets C,D). As a result, it was not possible to measure $R^Q(D_+D_z + D_zD_+)$ and $R^Q(3D_z^2\text{-}2)$ of D^α nuclei in ubiquitin within a reasonable time frame. Nevertheless, we were able to quantify the $R^Q(D_+D_z + D_zD_+)$ and $R^Q(3D_z^2\text{-}2)$ rates in a more concentrated sample of a smaller protein, GB1. Figure 4 shows that the inequalities $(5/3)R^Q(3D_z^2\text{-}2) \geq R^Q(D_z)$ (Figure 4a) and $(5/3)R^Q(D_+D_z + D_zD_+) \geq R^Q(D_+)$ (Figure 4b) are indeed satisfied without a single exception in GB1 at 22 °C, representing a useful semiquantitative consistency test of the experimental raw data. The profiles of $R^Q(D_+)$, $R^Q(D_z)$, and ^{15}N R_2,R_1 rates measured in GB1 are compared in Figure S1 of the Supporting Information. Notably, the flexibility of the backbone in the loop between Gly^9 and Leu^{13} and the C-terminus of GB1 is "picked-up" by D^α relaxation data with decreased $R^Q(D_+)$ and $R^Q(D_+D_z+D_zD_+)$ rates in these regions (Figure 4b and Figure S1 of the Supporting Information). Unfortunately, the presence of two glycine residues (Gly^{38} and Gly^{41}) prevents the quantification of D^α rates in another flexible loop of GB1 extending from Asn^{37} to Gly^{41} that is apparent from ^{15}N R_1,R_2 rate profiles (Figure S1b).

As described above, fast ^{2}H spin-flips lead to on average 4- to 5-fold sensitivity losses in the $R^Q(D_+D_z + D_zD_+)$ and $R^Q(3D_z^2\text{-}2)$ experiments (Figure 1, insets C,D) compared to the $R^Q(D_+)$ measurements (Figure 1, inset A) in GB1 at 22 °C. This situation is similar to ^{2}H relaxation measurements in the sugar and base moieties of RNA reported earlier.[67] Because of low sensitivity of "rank-2" relaxation measurements and, as a result, substantial errors in the derived $R^Q(D_+D_z + D_zD_+)$ and $R^Q(3D_z^2\text{-}2)$ rates, these data have not been used in further analysis. Mainly for the same reasons, no attempt has been undertaken to measure the relaxation rate of the fifth double-quantum ^{2}H coherence, D_+^2, at D^α sites.

D^α Relaxation-Derived Diffusion Tensor Parameters. Prior to obtaining the ^{2}H-derived measures of backbone order, it is important to establish the diffusion parameters of the global molecular reorientation. In analogy to the case of ^{15}N relaxation in protein backbones, the ^{2}H R_2/R_1 ratio, $R^Q(D_+)/R^Q(D_z)$, is to a good approximation independent of the amplitude and time scale of rapid internal motions.[13,52] It therefore serves as a good measure of the rate at which the C^α−D^α vector reorients with global tumbling.[70] Table 1 compares the parameters of the

Table 1. Comparison of D^{α} $R^Q(D_+)/R^Q(D_z)$- and ^{15}N R_2/R_1-Derived Diffusion Tensor Parameters of Ubiquitin (10, 27, and 40 °C) and GB1 (22 °C)[a]

	$\tau_{c,eff}$ [b]	$D_\parallel/D_\perp$	θ [c]	ϕ [c]
ubiquitin (10 °C)	6.68 ± 0.03	1.28 ± 0.04	12 ± 4	-22 ± 12
	(6.92 ± 0.02)	*(1.23 ± 0.02)*	*(6 ± 2)*	*(−19 ± 5)*
ubiquitin (27 °C)	3.94 ± 0.03	1.22 ± 0.03	8 ± 3	-8 ± 12
	(4.16 ± 0.01)	*(1.18 ± 0.02)*	*(6 ± 2)*	*(−16 ± 4)*
ubiquitin (40 °C)	2.90 ± 0.02	1.26 ± 0.03	16 ± 2	-34 ± 14
	(2.98 ± 0.01)	*(1.23 ± 0.01)*	*(6 ± 1)*	*(−48 ± 8)*
GB1 (22 °C)	4.43 ± 0.02	1.45 ± 0.03	20 ± 6	-61 ± 26
	(4.42 ± 0.01)	*(1.39 ± 0.02)*	*(24 ± 1)*	*(−99 ± 8)*

[a] ^{15}N R_2/R_1-derived diffusion parameters are shown in parentheses and italics below the D^{α} $R^Q(D_+)/R^Q(D_z)$-derived values. The orientation of the unique axis of the axially symmetric diffusion tensor is specified in the inertial frame for both proteins. The inertia tensors and direction cosine values for $C^{\alpha}-H^{\alpha}$ and N−H bond vectors have been calculated using the coordinates of protonated X-ray structures of ubiquitin and GB1 with respective PDB accession codes 1ubq[50] and 2qmt.[51] Seven C-terminal residues of GB1 do not have crystallographic coordinates and have been excluded from the derivation of the diffusion tensor. See Materials and Methods for the details of diffusion tensor determination. [b] $\tau_{c,eff}$ is given in units of nanoseconds (ns). [c] Angles are given in degrees. The angle γ between the D^{α}- and ^{15}N-derived diffusion axes can be estimated using the relationship $\cos\gamma = \cos\theta_1 \cos\theta_2 + \sin\theta_1 \sin\theta_2 \cos(\phi_1 - \phi_2)$, where $\{\theta_i,\phi_i\}$ are the polar angles that define the mean orientations of the unique axes of the two compared diffusion tensors. These angles are equal to 6 (2, 10)° for ubiquitin at 10 (27, 40) °C and 14.5° for GB1 (22 °C).

(axially symmetric) diffusion tensors derived from D^{α} $R^Q(D_+)/R^Q(D_z)$ and ^{15}N R_2/R_1 ratios for ubiquitin at three temperatures (see Materials and Methods). Since the diffusion tensor of ubiquitin has a relatively low diffusion anisotropy, we have chosen to test whether the $R^Q(D_+)/R^Q(D_z)$ ratios can reproduce a significantly more anisotropic reorientation on the sample of GB1 modified at the C-terminus (Table 1). Figure S2 of the Supporting Information shows the plots of $R^Q(D_+)/R^Q(D_z)$ as a function of the angle α that each of the $C^{\alpha}-D^{\alpha}$ bond vectors subtends with respect to the unique axis of the diffusion tensor, along with the best fits of the data for GB1 (22 °C) and ubiquitin (27 °C). Although the D^{α}-derived orientations of the principal axes (polar angles θ and ϕ in the inertial coordinate frame) are less well-defined in comparison to ^{15}N-derived values, a good agreement between the ^{15}N- and D^{α}-derived tensors is observed in all cases. The ratios of $\tau_{c,eff} = (2D_\parallel + 4D_\perp)^{-1}$ values obtained at 10, 27, and 40 °C in ubiquitin are very close to those expected on the basis of the Stokes−Einstein relationship. Despite the fact that D^{α} relaxation rates in ubiquitin were obtained using a 3-fold more concentrated protein sample than that used for ^{15}N rates, the D^{α}-derived values of $\tau_{c,eff}$ in ubiquitin are somewhat lower (3.6, 5.6, and 2.8% at 10, 27, and 40 °C, respectively) than their ^{15}N-derived counterparts at the same temperature (Table 1). Interestingly, in a recent study, exchange-free, purely dipolar contributions to ^{15}N relaxation rates, R_{dd}, in ubiquitin were derived.[17] These exchange-free rates indicated the presence of nonzero R_{ex} contributions to ^{15}N $R_{1\rho}$ rates for many residues in ubiquitin.[17] This implies that D^{α} $R^Q(D_+)/R^Q(D_z)$ ratios that are not affected by chemical exchange to any significant degree might serve as more robust estimates of the global reorientation parameters in small proteins.

Choice and Estimation of D^{α} QCC Values. Although the value of D^{α} QCC is not needed for determination of the diffusion tensor, knowledge of its accurate value is of paramount importance for interpretation of D^{α} relaxation rates in terms of motional parameters. Several solid-state NMR studies have reported the values of QCC for aliphatic deuterons attached to sp^3-hybridized carbons ranging from 168 ± 2 to 174 ± 2 kHz.[71] Solid-state NMR measurements by Haeberlen and co-workers provided the QCC values of the two α-deuterons in zwitterionic glycine equal to 159.9 and 169.4 kHz.[72] The authors explained the large difference between the two values by formation of weak C−H···O hydrogen bonds leading to a decrease of QCC in one of the two α-deuterons. Notably, oxygen acceptors are located in an adjacent layer of glycine molecules[72]—a situation that cannot be encountered in solution. In another low-temperature liquid crystal NMR study, the QCC value obtained for deuterons in a CD_3 methyl group of toluene (165 kHz) has been compared to the QCC of deuterons in cyclohexane-d_{12} (174 ± 2 kHz). The two values can be brought into exact agreement if the tetrahedral angle θ of the methyl group is assumed to be equal to 111° instead of 109.5°.[73] Interestingly, using solution NMR techniques, Mittermaier and Kay determined the QCC value of deuterons in $^{13}CH_2D$ methyl groups of proteins equal to 167 ± 1 kHz assuming $\theta = 109.5°$.[55] What is effectively determined in this study is the product $P_2(\cos\theta)$QCC, where $P_2(x) = 0.5(3x^2 - 1)$ is the second-order Legendre polynomial. If the value of θ is increased by only 1°,[74] the methyl QCC increases to 174 kHz. We note here that what is normally determined in single-crystal NMR measurements (unless they are performed at very low temperatures) is the product $\sqrt{(S^2\text{QCC})}$, where S is the order parameter of local motions. Here, local motions are assumed to be axially symmetric, and S includes the effects of slow motions and (potentially small) contributions from "rocking" motions of the molecule relative to the crystal lattice. If S^2 is assumed to be equal to 0.95,[75,76] then the measurements by Haeberlen and co-workers in α-glycine[72] yield QCC = 173.8 kHz for the non-hydrogen-bonded deuteron.

To obtain an independent estimate of QCC of α-deuterons in proteins, we followed the approach of Mittermaier and Kay.[55] Briefly, in an oriented protein, during the period T in the pulse scheme of Figure 1 (inset A), the ^2H magnetization evolves according to[55,77]

$$D_y \rightarrow D_y \cos(\pi\nu_Q T) - \{D_x D_z + D_z D_x\} \sin(\pi\nu_Q T) \qquad (8)$$

where the quadrupolar splitting $\nu_Q = (3/4)\text{QCC}\langle 3\cos^2\theta - 1\rangle$, θ is the angle between the principal axis of the electric field gradient tensor and the magnetic field, and the brackets $\langle\ \rangle$ denote ensemble averaging. The relaxation rates of D_y and $(D_zD_x + D_xD_z)$ coherences are described by eq 1 (the rate of in-phase ^2H magnetization, R_I) and eq 6 (the rate of anti-phase ^2H magnetization, R_A), respectively. Including relaxation during the period T, the evolution of the D_y magnetization (detected in the end of the experiment) is described by[55]

(70) Grzesiek, S.; Bax, A. *J. Am. Chem. Soc.* **1994**, *116*, 10196–10201.
(71) Burnett, L. H.; Muller, B. H. *J. Chem. Phys.* **1971**, *55*, 5829–5831.
(72) Muller, C.; Schajor, W.; Zimmermann, H.; Haeberlen, U. *J. Magn. Reson.* **1984**, *56*, 235–346.
(73) Rowell, J. C.; Phillips, W. D.; Melby, L. R.; Panar, M. *J. Chem. Phys.* **1965**, *43*, 3442–3454.
(74) Ottiger, M.; Bax, A. *J. Am. Chem. Soc.* **1999**, *121*, 4690–4695.
(75) Henry, E. R.; Szabo, A. *J. Chem. Phys.* **1985**, *82*, 4753–4761.
(76) LiWang, A. C.; Bax, A. *J. Magn. Reson.* **1997**, *127*, 54–64.
(77) Sörensen, O. W.; Eich, G. W.; Levitt, M. H.; Bodenhausen, G.; Ernst, R. R. *Prog. Nucl. Magn. Reson. Spectrosc.* **1983**, *16*, 163–192.

$$D_y(T) = \frac{A}{2}\exp\left\{-\frac{(R_I + R_A)}{2}T\right\}\left[(1-\Delta)\exp\left\{\frac{\Omega}{2}T\right\} + (1+\Delta)\exp\left\{-\frac{\Omega}{2}T\right\}\right] \quad (9)$$

where $\Omega = \sqrt{[(R_I - R_A)^2 - 4\pi^2\nu_Q^2]}$ and $\Delta = (R_I - R_A)/\Omega$. In contrast to the study of methyl groups,[55] here, the average rate of magnetization decay, $(R_I + R_A)/2$, is 2- to 3-fold higher than the *maximal* achievable quadrupolar splitting ν_Q, making the analysis of the decay of D_y (eq 9) extremely unreliable except for a (small) subset of residues where ν_Q is close to its maximal value and the zero-crossing of the magnetization decay can be achieved experimentally. In a pf1 phage-aligned, highly concentrated sample of GB1 (see Materials and Methods), a small subset of 11 peaks has been chosen where the zero-crossing of the D_y magnetization decay is apparent and where the extraction of a reliable albeit inexact value of ν_Q is still feasible. Although for this subset of residues the condition $(2\pi\nu_Q)^2 \gg (R_I - R_A)^2$ is always satisfied, simulations using synthetic data and average R_I, R_A rates and ν_Q values for GB1 showed that the fitting of the decay function D_y to a simpler three-parameter expression with a single effective $(R_I + R_A)/2$ rate[78] would produce errors in the derived ν_Q values of 5−8%. We have chosen, therefore, to fit the decay curves to the full expression in eq 9 above with four variable parameters (R_I, R_A, A, and ν_Q). Two examples of such fits for Leu[12] and Asp[40] from the chosen subset of 11 peaks in GB1 are shown in Figure 5a,b.

The $^1D_{C\alpha H\alpha}$ RDC measured as described in Materials and Methods is expressed as $^1D_{C\alpha H\alpha} = -(\mu_0/4\pi)(\gamma_C\gamma_H h/4\pi^2 r_{C\alpha H\alpha}^3)\langle 3\cos^2\theta - 1\rangle$, where γ_i is the gyromagnetic ratio of nucleus i, μ_0 is the vacuum permeability constant, and r_{CH} is the distance between C^α and H^α nuclei. Figure 5c,d shows the results of $^1D_{C\alpha H\alpha}$ measurements for the same pair of residues in GB1 as in Figure 5a,b, respectively. As shown by Mittermaier and Kay for methyl groups, the ratio of $\nu_Q/^1D_{C\alpha H\alpha}$, taken for the same α position, is independent of magnetic alignment ($\langle 3\cos^2\theta - 1\rangle$) and local motions.[55] The QCC value can then be obtained from the $\nu_Q/^1D_{C\alpha H\alpha}$ ratio following the relationship

$$\mathrm{QCC} = \frac{1}{12}\frac{\mu_0\gamma_C\gamma_H h}{\pi^3 r_{C\alpha H\alpha}^3}\left(\frac{\nu_Q}{^1D_{C\alpha H\alpha}}\right) \quad (10)$$

Note that, unlike in the case of methyl groups,[54] according to eq 10, D^α QCC does not depend on dihedral angles. The correlation of the ^2H quadrupolar splitting ν_Q with the $^1D_{C\alpha H\alpha}$ dipolar coupling for the subset of 11 peaks in GB1 is shown in Figure S3 of the Supporting Information. Linear regression analysis of this correlation provided a slope of -5.66 ± 0.34 (Pearson $R = 0.979$) when the (statistically insignificant) intercept was fixed at zero. The sign of ν_Q cannot be determined using this procedure, and ν_Q values have been assumed to have a sign opposite to that of the measured $^1D_{C\alpha H\alpha}$. Using eq 10 and assuming a standard r_{CH} distance of 1.095 Å,[79−81] we obtain D^α QCC = 173.7 kHz. Notably, any effects of local dynamics are canceled out by taking the ratio of ν_Q and $^1D_{C\alpha H\alpha}$, allowing one to use the value of r_{CH} distance "uncorrected" for any type of local motions.[81]

The procedure described above for the derivation of QCC values of D^α deuterons is only semiquantitative due to large uncertainties associated with the derivation of ν_Q. From the variation of individual $\nu_Q/^1D_{C\alpha H\alpha}$ ratios for 11 peaks in GB1 and from propagated errors in (fitted) ν_Q and $^1D_{C\alpha H\alpha}$ values, we estimate the uncertainty obtained in D^α QCC measurements on the order of 6−8% (∼10−14 kHz). However, *on average* we have been able to obtain a value of D^α QCC that agrees quantitatively with the results of solid-state measurements in α-glycine if dynamics is taken into account (see above). In what follows, we therefore used a uniform value of D^α QCC = 174 kHz in all calculations. It is unlikely that the variation in individual $\nu_Q/^1D_{C\alpha H\alpha}$ ratios in GB1 reflects the actual variation in D^α QCC values in a protein rather than the uncertainties of the measurement. Although hydrogen bonding is known to significantly affect quadrupolar couplings of deuterons,[76] α-deuterons in proteins are unlikely to participate in sufficiently strong hydrogen bonds. Of note, DFT calculations of QCC values of aliphatic deuterons bound to sp^3-hybridized carbons show that QCC is a highly local parameter whose value is dependent almost exclusively on the choice of the r_{CD} bond length (N. R. Skrynnikov, personal communication).

Comparison of ^2H- and ^{15}N-Derived Backbone Order. Since commonly only two rates, $R^Q(D_+)$ and $R^Q(D_z)$, are available for the derivation of motional parameters of $C^\alpha-D^\alpha$ vectors in proteins, caution must be exercised in a model-free-type analysis of D^α relaxation data to avoid overinterpretation when the results are compared to ^{15}N-derived dynamics parameters. Therefore, we have chosen to fit the $R^Q(D_+)$ and $R^Q(D_z)$ rates first to the simplest possible motional model that excludes the term describing local motions in the spectral density function of eq 3 ($\tau' = 0$). The majority of the residues in ubiquitin could be fit using such a single-parameter ($S^2_{C\alpha D\alpha}$) spectral density function with 5% probability of exceeding χ^2.[82] If the χ^2 of the fit exceeded this level of confidence, the $R^Q(D_+)$ and $R^Q(D_z)$ rates were fit to the full expression in eq 3 with two variable parameters ($S^2_{C\alpha D\alpha}$ and τ_f). The resulting values of $S^2_{C\alpha D\alpha}$ in ubiquitin at 10, 27, and 40 °C versus residue numbers are shown with blue rectangles in Figure 6a−c. For convenience of comparison, we have included in the plots the values of S^2_{NH} derived from ^{15}N relaxation data (red circles in Figure 6a−c). Table S1 in the Supporting Information lists all the dynamics parameters obtained at D^α positions of ubiquitin at the three temperatures. Figure 7 shows the ribbon structure of ubiquitin, where the $H^\alpha(D^\alpha)$ atoms (Figure 7a) and HN atoms (Figure 7b) are color-coded according to the values of $S^2_{C\alpha D\alpha}$ and S^2_{NH}, respectively. Overall, lower $S^2_{C\alpha D\alpha}$ and S^2_{NH} values are observed in the loop region between residues Thr[7] and Lys[11], in the bend near the polyubiquitination site (residues Ala[46]-Lys[48]), and in several C-terminal residues.

$C^\alpha-D^\alpha$ bond vectors are motionally distinct from the N−H bond vectors, with ^2H-derived $S^2_{C\alpha D\alpha}$ values on average slightly higher than their S^2_{NH} counterparts in N−H amides, in agreement with several earlier molecular dynamics simulations[83,84] as well as NMR spin relaxation[85,86] and liquid crystal studies.[81] In particular, the average $S^2_{C\alpha D\alpha}$ values of 0.86 (0.85; 0.84) are obtained in ubiquitin at 10 (27; 40) °C for the full protein and

(78) Kuboniwa, H.; Grzesiek, S.; Delaglio, F.; Bax, A. *J. Biomol. NMR* **1994**, *4*, 871–878.
(79) Jeffrey, G. *Accurate molecular structures, their determination and importance*; Oxford University Press: Oxford, 1992.
(80) Demaison, J.; Wlodarczak, G. *Struct. Chem.* **1994**, *5*, 57–66.
(81) Ottiger, M.; Bax, A. *J. Am. Chem. Soc.* **1998**, *120*, 12334–12341.
(82) Bevington, P. R.; Robinson, D. K. *Data Reduction and Error Analysis for the Physical Sciences*; WCB/McGraw-Hill: New York, 1992.
(83) Palmer, A. G.; Case, D. A. *J. Am. Chem. Soc.* **1992**, *114*, 9059–9067.
(84) Fadel, A. R.; Jin, D. Q.; Montelione, G. T.; Levy, R. M. *J. Biomol. NMR* **1995**, *6*, 221–226.
(85) Dellwo, M. J.; Wand, A. J. *J. Am. Chem. Soc.* **1989**, *111*, 4571–4578.

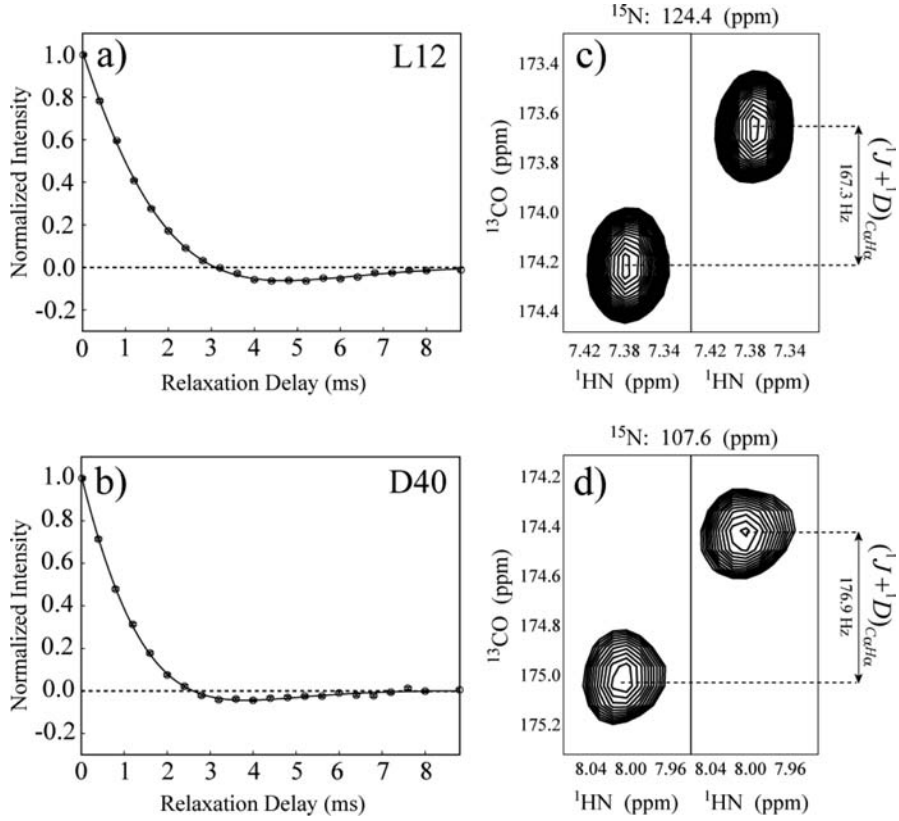

Figure 5. Examples of the decay curves for (a) Leu[12] and (b) Asp[40] of GB1 (22 °C) from the chosen subset of 11 peaks in GB1 that show clear-cut zero-crossing. The decay curves are fit to eq 9. Zero intensity is shown with a dashed line. The ^{1}HN−^{13}CO correlations obtained in the experiment of Yang et al.[56] allow the measurement of $^1D_{C\alpha H\alpha}$ residual dipolar couplings for (c) Leu[12] and (d) Asp[40]. The measured frequency differences ($^1J + {}^1D_{C\alpha H\alpha}$) are shown for each pair of peaks.

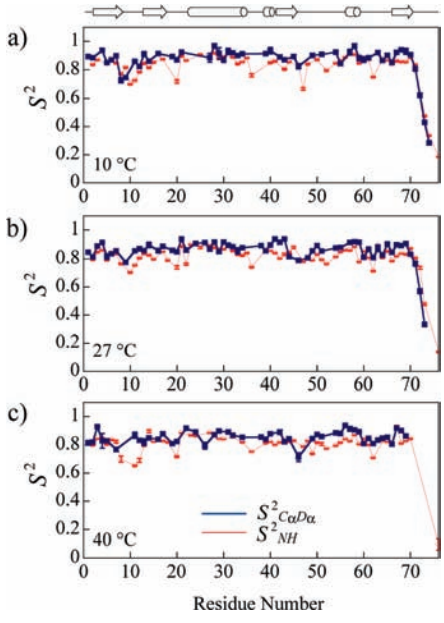

Figure 6. D$^\alpha$-derived $S^2_{C\alpha D\alpha}$ (blue rectangles and lines) and ^{15}N-derived S^2_{NH} (red open circles and lines) in ubiquitin at (a) 10, (b) 27, and (c) 40 °C, plotted as a function of protein sequence. Schematic representation of the secondary structure of ubiquitin is shown on top: β-sheets are depicted with arrows, while α-helices are represented with cylinders.

0.89 (0.87; 0.85) when the flexible C-terminal residues are excluded from analysis, while the respective average S^2_{NH} values are 0.82 (0.81; 0.81) for the full protein and 0.84 (0.83; 0.82) when the C-terminus is excluded. For those residues where both $S^2_{C\alpha D\alpha}$ and S^2_{NH} could be quantified, $S^2_{C\alpha D\alpha}$ values are higher than S^2_{NH} on average, with their respective average values of 0.86 (0.86; 0.85) and 0.82 (0.81; 0.80) at 10 (27; 40) °C. The difference in order parameters is even more pronounced in GB1. The values of $S^2_{C\alpha D\alpha}$ and S^2_{NH} in GB1 at 22 °C are plotted as a function of the protein sequence in Figure S4 of the Supporting Information. The higher rigidity of the C$^\alpha$−H$^\alpha$ (C$^\alpha$−D$^\alpha$) bond vectors in proteins is a consequence of the high correlation of their motions with those of the C$^\alpha$−C$^\beta$ bond vector of the same amino acid.[87] The latter anchors the side chain to the backbone, and thereby any reorientational motion will need to involve the bulk of the side chain. By contrast, the N−H^N amides are strongly affected by local crank-shaft-type motions of the peptide bond plane,[84,88] which involve anti-correlated modulations of the associated backbone φ_i and φ_{i-1} dihedral angles. There are notable exceptions to this general trend, however. For example, in the C-terminal region of ubiquitin following Leu,[71] average $S^2_{C\alpha D\alpha}$ (S^2_{NH}) = 0.61 (0.63) have been obtained at 27 °C, whereas the C-terminal residues in GB1 have average $S^2_{C\alpha D\alpha}$ (S^2_{NH}) = 0.22 (0.24). Interestingly, the D$^\alpha$ rates of the C-terminal residues in both proteins cannot be fit to the simplest ($S^2_{C\alpha D\alpha}$ only) Lipari−Szabo model because the increased $R^Q(D_z)$ rates at the C-terminus (Figure 3a−c) cannot be explained without invocation of fast local motions. In principle, direct comparison of $S^2_{C\alpha D\alpha}$ and S^2_{NH} on a per-residue basis can be ambiguous, since

(86) LeMaster, D. M.; Kushlan, D. M. *J. Am. Chem. Soc.* **1996**, *118*, 9255–9264.
(87) Brüschweiler, R. *J. Chem. Phys.* **1995**, *102*, 3396–3403.
(88) Brüschweiler, R.; Wright, P. E. *J. Am. Chem. Soc.* **1994**, *116*, 8426–8427.

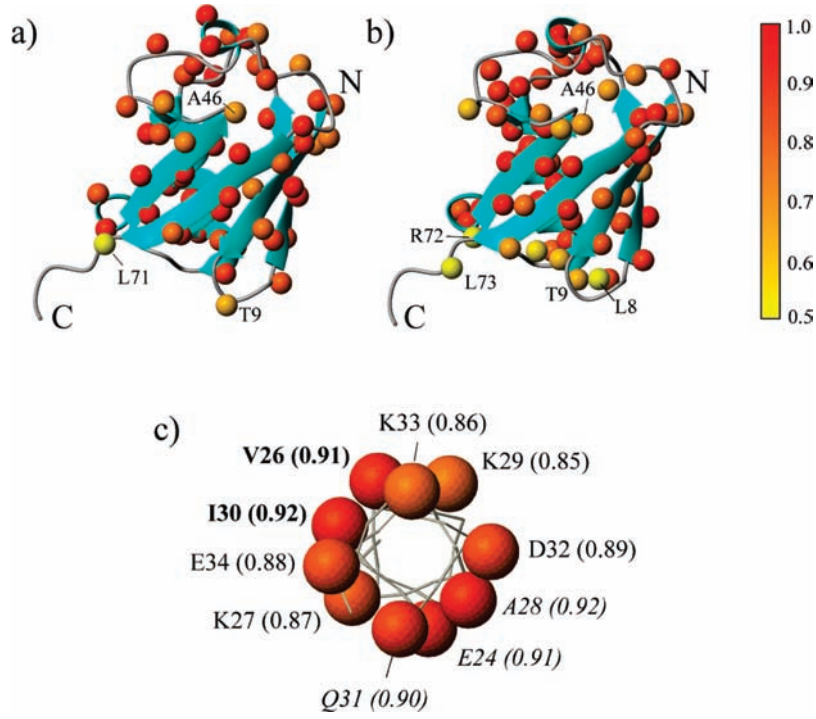

Figure 7. Ribbon diagrams of ubiquitin crystal structures with (a) D^α and (b) HN atoms represented as balls color-coded according to the values of $S^2_{C\alpha D\alpha}$ and S^2_{NH} (27 °C), respectively. The elements of the secondary structure are shown in blue. The placement of a number of residues discussed in the text is indicated with residue numbers. (c) Schematic representation of the α-helical stretch of ubiquitin (residues Ile^{23}-Glu^{34}) viewed from the top along the helical axis. The color-coded balls represent D^α atoms. The values of $S^2_{C\alpha D\alpha}$ are listed along with residue numbers. $S^2_{C\alpha D\alpha}$ values of residues with $C^\alpha-D^\alpha$ vectors directed toward a short 3_{10}-helical stretch (Pro^{38}-Gln^{40}) are shown in bold, whereas those directed toward the interior of the protein core on the other side of the α-helix are shown in italics. The color-coding scale is shown to the right of panel b. The diagrams have been generated using the program Molmol.[89]

higher S^2_{NH} values may result from the use of different motional models for the derivation of $S^2_{C\alpha D\alpha}$ and S^2_{NH} as well as significantly different time scales of N−H and $C^\alpha-D^\alpha$ bond vector fluctuations. Furthermore, since their respective diffusion tensor parameters have been used for the derivation of $S^2_{C\alpha D\alpha}$ and S^2_{NH}, any small differences in these parameters (Table 1) can skew the differences between $S^2_{C\alpha D\alpha}$ and S^2_{NH} ($S^2_{C\alpha D\alpha} - S^2_{NH}$) in favor of somewhat smaller values, adding additional uncertainty to direct comparisons of backbone order at the amide and D^α sites (*vide infra*).

Since different motional processes are sampled by D^α and ^{15}N relaxation rates, it would be of interest to compare the degree of backbone order in the elements of protein secondary structure where $C^\alpha-H^\alpha(D^\alpha)$ and N−H bond vectors are oriented in different directions. For example, ^{15}N relaxation data do not sample fast local motions that occur around the helical axis, such as a rolling motion of an α-helical shaft,[90] because in α-helices all N−H bonds lie approximately parallel to the helical axis, forming hydrogen bonds with a carbonyl oxygen acceptor of residue $i - 4$. In contrast, $C^\alpha-H^\alpha(D^\alpha)$ bond vectors are directed outward, making angles of up to ∼70° with the α-helical axis. Interestingly, in the α-helical segment of ubiquitin (residues Ile^{23}-Glu^{34}), $S^2_{C\alpha D\alpha}$ are noticeably higher for the residues whose $C^\alpha-H^\alpha(D^\alpha)$ bond vectors are directed toward a short 3_{10}-helical stretch in the protein structure (Val^{26}, Ile^{30}) or oriented toward the interior of the protein at the other face of the α-helix (Glu^{24}, Ala^{28}, Gln^{31}). Figure 7c shows a schematic representation of the α-helix in ubiquitin viewed from its N-terminal end approximately along the axis of the helix, with $S^2_{C\alpha D\alpha}$ (27 °C) shown for each D^α site. In GB1, the residues of the α-helix (Ala^{23}-Asp^{36}) facing the hydrophobic interior of the protein (Ala^{26}, Phe^{30}, Tyr^{33}, and Ala^{34}) also tend to have elevated $S^2_{C\alpha D\alpha}$. The resulting alternating patterns of $R^Q(D_+)$ rates (Figure 3d−f and Figure S1 of the Supporting Information) and $S^2_{C\alpha D\alpha}$ values (Figure 6a,b and Figure S4 of the Supporting Information) are apparent in the helical regions of both proteins, indicating that the backbone order as probed by ^{2}H spin relaxation at D^α positions is likely to be related to the tightness of hydrophobic packing in protein cores. Specifically, the values of $S^2_{C\alpha D\alpha}$ in the α-helix of ubiquitin (Figure 7c) are weakly but statistically significantly correlated with the buried surface area and the hydrophobic contact potential[91,92] at C^α positions (Pearson $R >$ 0.5). We note that the "zigzag" patterns of $R^Q(D_+)$ rates and the resulting $S^2_{C\alpha D\alpha}$ values cannot be explained by the anisotropy of the global molecular tumbling, as the unique diffusion axis of ubiquitin subtends an angle of only ∼10° relative to the α-helical axis.

Molecular Dynamics Simulations and Alternative Analyses of D^α ^{2}H Rates. To gain more confidence in the ^{2}H-derived measures of backbone order, we have performed molecular dynamics simulations for ubiquitin at 27 °C (see Materials and Methods). Interestingly, the best agreement between MD-derived $S^2_{C\alpha H\alpha}$ and experimental $S^2_{C\alpha D\alpha}$ order parameters is achieved when the D^α QCC value is (slightly) lowered to 171 kHz. A comparison between experimental $S^2_{C\alpha D\alpha}$ (QCC = 171 kHz) and

(89) Koradi, R.; Billeter, M.; Wüthrich, K. *J. Mol. Graphics* **1996**, *14*, 51–55.
(90) Fischer, M. W. F.; Zeng, L.; Majumdar, A.; Zuiderweg, E. R. P. *Proc. Natl. Acad. Sci. U.S.A.* **1998**, *95*, 8016–8019.
(91) Lee, B.; Richards, F. M. *J. Mol. Biol.* **1971**, *55*, 379–400.
(92) Kurochkina, N.; Lee, B. *Protein Eng.* **1995**, *8*, 437–442.

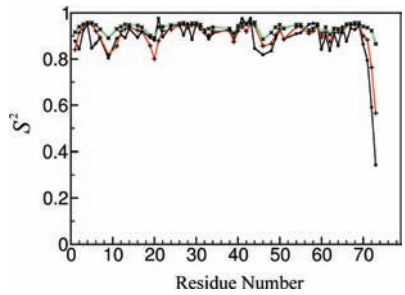

Figure 8. Experimental $S^2_{C\alpha D\alpha}$ order parameters of ubiquitin at 27 °C (black line with closed circles) determined using a uniform QCC value of 171 kHz, in comparison with the MD-derived $S^2_{C\alpha H\alpha}$ values obtained from a 1 μs MD trajectory of ubiquitin averaged over 1 ns (green line with × symbols) and 5 ns (red line with + symbols) time windows. See Materials and Methods for the details of MD simulations.

MD-derived $S^2_{C\alpha H\alpha}$ values obtained using a 1 μs MD trajectory of ubiquitin averaged over 1 and 5 ns time windows is shown in Figure 8. A good agreement is found for the loop region of the N-terminal β-hairpin and the flexible C-terminus. The experimentally observed decrease in the order parameters of loop residues Ile[44], Ala[46], Lys[48], and Glu[49], whose side chains point toward the solvent, is well reproduced by the MD simulation. Furthermore, the "zigzag" pattern displayed by the experimental $S^2_{C\alpha D\alpha}$ values in the Tyr[59]-Lys[63] loop is also clearly observable in the simulation profile (Figure 8). For this region, the order parameters directly reflect the orientation of the associated side chain, with lower S^2 for inward-oriented side chains and higher S^2 for more solvent-exposed ones. Lys[63] is a notable exception with a relatively high $S^2_{C\alpha H\alpha}$ despite its high solvent accessibility. The close relationship between $S^2_{C\alpha D\alpha}$ and the associated side-chain properties is corroborated by the very close agreement between $S^2_{C\alpha D\alpha}$ and $S^2_{C\alpha C\beta}$ values found in the MD simulation of ubiquitin (see Supporting Information, Figure S6).

The comparisons of ^{15}N- and ^{2}H-derived measures of backbone order described here have been performed using the respective (^{15}N-derived or ^{2}H-derived) overall diffusion tensor parameters (Table 1). Obviously, there is a unique diffusion tensor that characterizes the rotational reorientation of a molecule. Therefore, it would be of interest to ascertain that the relation between $S^2_{C\alpha D\alpha}$ and S^2_{NH} noted above holds if analysis is performed using a common set of diffusion tensor parameters for both nuclei. We have repeated the analysis as described in the "Comparison of ^{2}H- and ^{15}N-Derived Backbone Order" section above for ubiquitin at 27 °C using common diffusion tensor parameters for ^{15}N and ^{2}H data with the averaged values of $\tau_{c,eff} = (2D_{||} + 4D_{\perp})^{-1} = 4.05$ ns; $D_{||}/D_{\perp} = 1.20$; $\theta = 7°$; $\phi = -12°$, and D$^\alpha$ QCC = 171 kHz as obtained from MD simulations. The results of this analysis are presented in Figure S5 of the Supporting Information. The main conclusions obtained in the case when separate diffusion tensors have been used remain in force. In particular, the average $S^2_{C\alpha D\alpha}$ (S^2_{NH}) values of 0.87 (0.84) are obtained for all residues of ubiquitin, while $S^2_{C\alpha D\alpha}$ (S^2_{NH}) values of 0.89 (0.86) are obtained when the flexible C-terminal and loop regions are excluded from analysis. However, when the same analysis (common diffusion tensor, QCC = 171 kHz) is performed for GB1, a number of residues give $S^2_{C\alpha D\alpha}$ values higher than the theoretical limit of unity. When the D$^\alpha$ QCC value is "reset" to 174 kHz, the relationship between $S^2_{C\alpha D\alpha}$ and S^2_{NH} still holds in both proteins, although the average $S^2_{C\alpha D\alpha}$ values become only insignificantly higher than S^2_{NH} in ubiquitin.

Concluding Remarks. In summary, we have shown that deuterium relaxation rates measured at deuterated carbon-α positions (D$^\alpha$) serve as robust measures of backbone order in proteins. D$^\alpha$ relaxation rates are straightforward to interpret in terms of motional parameters ($S^2_{C\alpha D\alpha}$, τ_f), provided that a uniform quadrupolar coupling constant (QCC) is assumed for all D$^\alpha$ sites in the protein molecule. To the best of our knowledge, this is the first attempt to use ^{2}H relaxation as a probe of backbone dynamics in proteins. Clearly, the experiments developed for D$^\alpha$ relaxation rate measurements are not sufficiently sensitive for routine applications requiring the use of concentrated [U-^{2}H,^{13}C,^{15}N]-labeled protein samples. Most of the D$^\alpha$ relaxation measurements described in this work have been performed on 3.2 mM [U-^{2}H,^{13}C,^{15}N]-ubiquitin using a room-temperature probe. Obviously, at such high protein concentrations, potential aggregation of protein molecules in NMR samples is of concern. The data on diffusion tensor characteristics summarized in Table 1 show that this is apparently not the case for both proteins studied in this work. With the increased sensitivity of NMR measurements due to the continuing development of cryogenically cooled detection devices and the availability of higher magnetic fields, we anticipate that $R^Q(D_+)$, $R^Q(D_z)$ measurements would become feasible on protein samples with regular protein content (0.5−1.0 mM). Moreover, with the *increasing* molecular weight of a protein under study, ^{2}H spin-flipping rates would *decrease* (Figure 3a−c). Therefore, the methods described in this work may be applicable to well-behaved medium-sized proteins (up to ∼200 residues), as the sensitivity of the experiment in Figure 1 is primarily determined by the rate of ^{2}H spin-flips at the step when the magnetization is transferred from ^{13}C$^\alpha$ spins to D$^\alpha$ and back.

For sensitivity reasons, because of the requirement for [U-^{2}H,^{13}C,^{15}N] labeling, and because less data are available per nuclear probe in the case of D$^\alpha$ measurements at a single spectrometer field ($R^Q(D_+)$, $R^Q(D_z)$ rates versus ^{15}N R_1, R_2 and ^{1}H−^{15}N NOEs), the developed methodology is not meant to substitute for the commonly used ^{15}N amide nuclei as NMR spin probes of backbone dynamics. Rather, it can be envisaged to serve as a useful complement to existing, more sensitive techniques. Indeed, it should be kept in mind that the D$^\alpha$ relaxation rates measured in this work sample motions occurring in the protein backbone at positions that are distinct—chemically, structurally, and motionally—from those normally sampled by conventional ^{15}N-based techniques. This work represents an attempt to get an alternative view of dynamic processes in protein molecules and to establish the range of applicability and utility of the described NMR methodology. In this context, it is noteworthy that, in principle, the measurements of ^{13}C$^\alpha$ relaxation in proteins[93,94] would provide the same information about backbone dynamics in a protein molecule as the D$^\alpha$ methodology described here. The use of (protonated) carbon-α probes would, however, suffer from the same set of shortcomings and uncertainties as ^{15}N-based methods (uncertainty in ^{13}C$^\alpha$−H$^\alpha$ distances, site-specific ^{13}C CSA variation, contributions to ^{13}C relaxation from dipolar interactions with ^{13}C$^\beta$ and ^{13}CO spins, *etc.*). We have chosen to compare the D$^\alpha$-derived motional parameters with more commonly used ^{15}N spin probes. An NMR study that quantifies ^{13}C$^\alpha$ relaxation rates in selectively ^{13}C$^\alpha$-enriched protein samples[95] and compares the measures of

(93) Lee, L. K.; Rance, M.; Chazin, W. J.; Palmer, A. G. *J. Biomol. NMR* **1997**, *9*, 287–298.
(94) Idiyatullin, D.; Nesmelova, I.; Daragan, V.; Mayo, K. H. *Protein Sci.* **2003**, *12*, 914–922.

backbone order thus obtained with the D^α-derived data reported here is in progress.

Acknowledgment. This work has been supported in part by the General Research Board (GRB) Award to V.T. from the University of Maryland. The authors are grateful to Dr. Pramodh Vallurupalli and Prof. Lewis Kay (University of Toronto, Canada) for useful discussions, Dr. Andy Byrd (NCI, Federick, Maryland) for the generous gift of [U-^{15}N,^{13}C,^{2}H]-ubiquitin used in this work, Dr. Chenyun Guo (University of Maryland) for preparation of [U-^{15}N,^{13}C,^{2}H]-GB1 and [U-^{15}N]-GB1 samples, Prof. David Fushman (University of Maryland) for providing the sample of [U-^{15}N]-ubiquitin and the Matlab-based software for ^{15}N relaxation data analysis, and Prof. Nikolai Skrynnikov (Purdue University, West Lafayette, IN) for sharing with us some unpublished results of DFT calculations of quadrupolar coupling constants.

(95) Lundström, P.; Teilum, K.; Carstensen, T.; Bezsonova, I.; Wiesner, S.; Hansen, D. F.; Religa, T. L.; Akke, M.; Kay, L. E. *J. Biomol. NMR* **2007**, *38*, 199–212.

Supporting Information Available: Figure S1, D^α $R^Q(D_+)$, $R^Q(D_z)$ relaxation rate profiles along with ^{15}N R_1, R_2 profiles in GB1 at 22 °C as a function of the protein sequence; Figure S2, dependence of $R^Q(D_+)/R^Q(D_z)$ on the angle α formed by $C^\alpha-D^\alpha$ bonds and the principal axis of the diffusion tensor in GB1 at 22 °C and in ubiquitin at 27 °C; Figure S3, correlation plot of the D^α quadrupolar splittings, ν_Q, and $^1D_{C\alpha H\alpha}$ residual dipolar couplings measured for a subset of 11 peaks in the oriented sample of GB1; Figure S4, $S^2_{C\alpha D\alpha}$ and S^2_{NH} as a function of sequence for GB1 at 22 °C; Figure S5, $S^2_{C\alpha D\alpha}$ and S^2_{NH} for ubiquitin at 27 °C obtained using a common diffusion tensor and QCC = 171 kHz; Figure S6, agreement between $S^2_{C\alpha H\alpha}$ and $S^2_{C\alpha C\beta}$ values found in the 1-μs MD simulation of ubiquitin at 27 °C; table listing $S^2_{C\alpha D\alpha}$ and τ_f values obtained in ubiquitin at 10, 27, and 40 °C. This material is available free of charge via the Internet at http://pubs.acs.org.

JA9063958